MEASURING BROADBAND, ULTRAWEAK, ULTRASHORT PULSES

A Dissertation
Presented to
The Academic Faculty

by

Aparna Prasad Shreenath

In Partial Fulfillment
of the Requirements for the Degree
Doctor of Philosophy

School of Physics
Georgia Institute of Technology
August 2005

MEASURING BROADBAND, ULTRAWEAK, ULTRASHORT PULSES

Approved by:

Dr. Rick Trebino, Advisor
School of Physics
Georgia Institute of Technology

Dr. T. A. Brian Kennedy
School of Physics
Georgia Institute of Technology

Dr. Phillip First
School of Physics
Georgia Institute of Technology

Dr. John A. Buck
School of Electrical and Computer Engineering
Georgia Institute of Technology

Dr. Stephen E. Ralph
School of Electrical and Computer Engineering
Georgia Institute of Technology

Date Approved: 29 June 2005

DEDICATION

To my late grandmother, Vaidehi, "Akka" as I used to call her, for providing the inspiration ... and to my husband, Jay, for making sure I didn't skimp on the other 99%.

ACKNOWLEDGEMENTS

I would like to take this opportunity to thank some of the many people for making this dissertation possible.

Let me start off by thanking my advisor, Prof. Rick Trebino, for giving me the opportunity to work on some very interesting and challenging problems. He not only provided constant motivation and encouragement to be resourceful in the laboratory, but also helped me hone my skills in giving presentations, writing papers and participating in team work. Thanks to him also for providing the opportunity to present at the many conferences, and for getting to meet so many brilliant researchers in various related fields at these conferences, and also at the special group meetings.

Mark Kimmel patiently taught me everything about working in a laboratory, to enjoy working with my hands and being an experimentalist. I am also very indebted to him for staying back with me late those evenings when I searched for the elusive signal, and then walking me over to my car safely, because he didn't want me walking alone on campus that late. I owe Dr. Erik Zeek a great deal for his tolerance in answering all my "dumb" questions patiently and helping me back into the answers, and for those pep-talks that boosted my self-confidence enormously. Special thanks to Dr. Xun Gu for being a pal, colleague and councillor - for always having my back. Thanks to Stephan, Wenyu, Xuan, Selçuk, Kristen and Pablo, who worked with me closely on various projects and who taught me a lot in their own different ways. And finally thanks to all members of the FROG team for making the lab a pleasant place to work in, a home away from home. Thanks to Linda Trebino for easing the paperwork burden on us grad students and also for those relaxing pizza-and-movie nights that allowed the FROG team to get to know each other informally. Thanks also to my fellow classmates David Kulp, Denis Semwogerere and Barbara Breen, and my room-mate, Tahirih Lackey for being my support net outside my research group.

I am especially grateful for the support provided by my parents, Keshav Prasad and Vijaya Shree Prasad, and for my grandmother, Akka, for encouraging me to pursue my

dreams of being a physicist from childhood, and for providing me with the opportunity to do so. Their love and faith in me have kept going. Many thanks to my brother, Suparna for keeping my feet grounded at all times. I am also grateful for the support and encouragement provided by my parents-in-law, Shreenath and Bhargavi - for being proud of who I am and what I do.

Most important of all, I owe everything to my love, my friend and my husband, Jay. He has been there to encourage, rationalize and bully me through the dark moments and to celebrate the good ones. His cheerful patience and philosophy of "*It's all good, baby!*" has seen me through my long years in grad school. He deserves this day as much as I do. Jay, thank you! *I love you!*

TABLE OF CONTENTS

LIST OF FIGURES

SUMMARY

Many essential processes and interactions on atomic and molecular scales occur at ultrafast timescales. The ability to measure and manipulate ultrashort pulses hold the key to probing and understanding these key processes that physicists, engineers, chemists and biologists study today. Measuring ultrashort pulses means that we measure both the intensity (which is a function of time) *and* the phase of the pulse in time. Or alternately we might measure spectrum and spectral phase (in the corresponding Fourier domain). In the early 1990's, the invention of FROG opened up the field of ultrashort measurement with it's ability to measure the complete pulse. Since then, there have been a whole host of pulse measurement techniques that have been invented to measure all sorts of ultrashort pulses. However, no variation of FROG *nor any other fs pulse measurement technique*, for that matter, has yet been able to completely measure arbitrary ultraweak femtosecond light pulses such as those found in nature.

In this thesis, we will explore a couple of highly sensitive methods in a quest to measure ultraweak ultrashort pulses. We explore the use of Spectral Interferometry, a known sensitive technique as one possibility. We find that it has certain drawbacks that make it not necessarily suitable to tackle this problem. But in the course of our quest, we find that this technique is highly suitable for measuring 10s of picosecond-long shaped pulses. We discuss a couple of developments which make SI highly practical to use for such shaped pulse-measurements.

We also develop a new technique which is a variation of FROG, based on the nonlinearity of Difference Frequency Generation and Optical Parametric Amplification, which can amplify pulses as weak as a few hundred attojoules to be able to spectrally resolve them and measure the full intensity and phase of these pulses. This technique offers great potential to measure generalized ultraweak ultrashort pulses.

CHAPTER 1

INTRODUCTION AND SCOPE

Ultrafast (or ultrashort) laser pulses are the shortest events ever created. Although the term typically refers to femtosecond (fs) pulses, it is now possible to generate and measure attosecond (as) pulses - the next new frontier. Ultrashort pulses have large bandwidths, as a consequence of the Heisenberg Uncertainty Principle. These pulses can be defined by their electric fields as a function of space and time. They have both amplitude as well as phase. Because they are squeezed into such short durations, even modest ultrashort pulses (50 fs long with 1mJ average energy) have extremely large peak powers ($\simeq$ 20GW). During one fs, visible light travels about 300 nm the distance of several thousand elementary cells in a solid, a sizable distance in atomic scales.

Why do we care about ultrashort pulses and their measurement? Well, for one thing, most essential processes and interactions on atomic and molecular scales occur at ultrafast timescales. For instance, in the Hydrogen atom, the period of revolution of an electron in a high Rydberg state of $n = 10$ is found to be 150 fs. Life-times of highly excited states in molecules, electron-hole pair relaxation times are all ultrafast. Exotic biological processes like photosynthesis, vision and protein-folding, to name a few, have events occurring on fs timescales. Collisions in room temperature liquids, molecular vibrations, re-orientations and other processes studied by chemists have fs signatures. Attosecond physics involves sub-atomic distances and extremely intense energies.

The ability to measure and manipulate ultrashort pulses hold the key to probing and understanding many key processes that physicists, engineers, chemists and biologists study today.

What do we mean by ultrashort pulse measurement? We can use photo-detectors and measure the average power of an ultrashort pulse. And we could use spectrometers and measure its spectrum. But this does not mean that we have "measured" the ultrashort

pulse. As we mentioned before, the electromagnetic field envelope is a complex quantity. It is not just enough to know intensity (which is a function of time) but we require the phase of the pulse in time, as well. Or alternately we might measure spectrum and spectral phase (in the corresponding Fourier domain). A spectrum tells us what colors (or wavelengths) are present in the ultrashort pulse. The phase tells us when or in what order the color occurred. A very simplistic way of saying what this means is that this knowledge of spectrum and phase can be used to track down the sequence of events occurring in the process under study, when the light pulse was emitted.

Even as recently as the early 1990s, the problem of ultrashort pulse measurement was an unsolved problem. Sure, intensity autocorrelators were used to "measure" the ultrashort pulses. But since no shorter event than an ultrashort pulse was available, autocorrelators used the pulse to measure itself. This resulted in getting a smeared out version of the pulse. While this gave an idea of the pulse length, it was still susceptible to ambiguities and errors. Despite this, intensity autocorrelators were the most common method of measuring ultrashort pulses for over 25 years for lack of better methods, and is still used today by some die-hard researchers.

Then in 1993, progress was suddenly made by the invention of Frequency-Resolved Optical Gating (FROG) [39, 38], a spectrally resolved version of the autocorrelator. An iterative algorithm [40, 25] was used to extract a unique solution the *only* field that could have produced the measured signal. It was now possible to measure the complete time-dependent electric field, that is, the time-dependent intensity and phase, of a single ultrashort laser pulse in different sort of situations. Soon thereafter, variations of FROG were discovered [38]. Complex pulses and pulses as short as 4.5 fs in length, could be measured using FROG [1] or its variations. Even more interestingly, a pulse could be characterized by a FROG-like technique and then used as a reference pulse for another technique, such as a Cross-correlation FROG [28] or Spectral Interferometry [19] to measure a different pulse. Pretty soon there was a glut of ultrashort pulse measurement techniques to measure all kinds of exotic ultrashort pulses. This opened up fields of research and ideas that had not been considered possible before. One such idea was to be able to measure arbitrary ultrashort

light pulses. And not just any ultrashort pulses, but extremely weak - **ultraweak, ultrashort** pulses. For, no variation of FROG nor any other fs pulse measurement technique, for that matter, had yet been able to completely measure general ultraweak femtosecond light pulses. That has been the goal of this study.

In this thesis, we will explore a couple of sensitive methods in a quest to measure ultraweak ultrashort pulses.

First of all, in Chapter 2, I will discuss FROG in some detail and go on to talk about the direction-of-time ambiguities in Second Harmonic Generation (SHG) FROG. This resulted in a new modification of SHG FROG called the Procedure for Objectively Learning the Kalibration And Direction Of Time (POLKADOT) FROG [45]. The technique involves replacing the beam-splitter in a multi-shot FROG device with an etalon of known spacing. Since the trailing pulses from the multiple pulse train generated in the etalon will always be weaker than the first "direct" pulse, POLKADOT FROG eliminates the direction of time ambiguity. As a slight modification, placing the etalon in the beam path before the pulse enters the FROG device allows painless temporal and spectral calibration of even single-shot FROG devices. In fact, POLKADOT FROG in this form is routinely used in the calibration of Swamp Optics GRENOUILLEs and it is hoped that it is used in other laboratories as well.

In Chapter 3, we will look into the first technique mentioned for measuring arbitrary weak pulses. It is a technique called Spectral Interferometry that has been around since the 1970s [20, 32], but was first demonstrated using a TADPOLE algorithm in 1995 by Fittinghoff et. al [19]. This technique is a linear heterodyne technique which is extremely sensitive, capable of measuring pulses as weak as 42×10^{-21} J. Initially, we tinker with this technique and try to simplify its experimental set-up by making it alignment-free. We show that even with a mis-alignment of as much as 32°, we are still able to measure the intensity and phase of a pulse accurately. We use a known double pulse as our test case for this alignment-free spectral interferometric experiment. Next, we show that we can perform the same spectral interferometric experiment by replacing the beam-splitter by a 2×2 fiber-coupler and still extract the same information. This device would be very

versatile and portable and could be used for a wide variety of pulses ranging from the few femtosecond durations up to 10s of picosecond durations, depending on the spectrometers available to measure such pulses. We will also discuss our brief exploration of using spectral interferometry to study a general light pulse, the ultrafast fluorescence emitted by the laser dye, Malachite Green and the problems we encountered in using this technique for such a measurement which eventually led us to find a new technique to measure such pulses.

In Chapters 4 and 5, we will discuss a new variation of FROG, which we call Optical Parametric Amplification Cross-correlation FROG (OPA XFROG) [48, 22] which showed that it could overcome the drawbacks of Spectral Interferometry, while at the same time providing extremely high sensitivity for measuring weak pulses. OPA XFROG is a non-linear technique based on the process of parametric generation, during the 3-wave mixing process of Difference Frequency Generation. During this process, the weak signal under study experiences exponential gain [6, 35, 47], and can then be spectrally resolved in order to measure its intensity and phase. Since this is a new variation of XFROG, we first show the reliability of this technique by comparing it with a well known technique and then go on to make measurements of pulses as weak as a few hundred attojoules. This technique is slightly more sensitive than spectral interferometry and promises to be a suitable technique to measure ultraweak spatially incoherent pulses. We go on to show that it is possible to make simultaneous broadband measurements of these ultrashort pulses without having to modify the phase-matching crystal angles. This makes OPA XFROG a very simple device which can be made to measure extremely weak pulses in an automated manner.

Chapter 6 will contain conclusions and future directions on the various techniques discussed in this thesis.

CHAPTER 2

FREQUENCY RESOLVED OPTICAL GATING AND THE DIRECTION OF TIME AMBIGUITY

Sections of this chapter originally appeared as a paper by the author:

E. Zeek, A. P. Shreenath, P. O'Shea, M. Kimmel, and R. Trebino, "Simultaneous automatic calibration and direction-of-time removal frequency-resolved optical gating," Applied Physics B-Lasers and Optics 74, S265-S271 (2002). [45]

2.1 A very brief summary to Frequency Resolved Optical Gating

A decade ago, the measurement, characterization and representation of ultrashort laser pulses was a challenging task. The problem was that the temporal length of the ultrashort pulse was too short to use any of the conventional detection methods to measure its length. Yet, the bandwidth of the pulse was so large that it was no longer just sufficient to measure the intensity of the pulse - its phase had to be measured as well. Then, in the early 1990s, a new technique was proposed to measure such pulses. The measurement took place in the simultaneous *time-frequency domain* to result in a *spectrogram* of the pulse. From such a spectrogram, the intensity and phase of the pulse could be retrieved easily. In this way, it was possible to characterize the pulse completely. This technique was called **Frequency Resolved Optical Gating (FROG)** [38, 39]. FROG relied on nonlinear optical properties of material media for the above measurements.

In FROG, a nonlinear process is used to gate the unknown pulse in the time domain with a time-delayed replica of the same pulse. The signal resulting from such a nonlinear process is then spectrally resolved (usually with the help of a spectrometer) to result in the FROG trace, which is, in fact a spectrogram. Unlike in a usual spectrogram (which requires a known gate pulse), however in FROG, although the gate function may be unknown, it

is still possible to extract the intensity - and more importantly, the phase of the pulse. This is attributed to the existence of a **unique** solution to the problem of *two-dimensional phase-retrieval.* This inversion problem is a well-known **solved** problem of phase-retrieval in the field of image-science.

FROG is a general technique which can use nearly any fast nonlinear optical process for its measurement. Due to its generality, it has been successful in measuring a wide variety of pulses, in various ultrafast domains.

Interpretation of the FROG trace is extremely intuitive. The intensity and phase of a pulse can be estimated just by looking at a FROG trace. However, FROG uses iterative algorithms to rigorously measure the intensity and phase of a pulse. The iterative algorithms are very fast, typically running over 100 iterations, in a matter of a few seconds. This is typically all that is needed to get a good convergence. Newer inversion algorithms now available commercially can even be used in real time to measure pulses.

The FROG retrievals of pulses are extremely accurate, so much so that the algorithm actually quantizes the error in measurement. Typical pulse measurements have less than 0.5% error. This is possible because the FROG algorithm incorporates a feedback mechanism to check the validity of the measured data. The measured FROG trace contains N $\times$ N measured points, grossly over-determining the net 2N intensity and phase points that are needed for complete pulse characterization. Systematic errors in the measurement can be detected if the algorithm does not converge and if the FROG error is large. These errors can either be modelled into the FROG algorithm, or eliminated in the preprocess stage of the retrieval [25].

Another powerful feedback mechanism in FROG is the capability of computing the frequency and delay marginals of the trace. These marginals correspond to the measured spectrum and autocorrelation of the pulse respectively. Direct comparisons between these quantities can then be used to correct for and/or improve FROG retrievals.

As long as the pulse spectrogram is completely contained within the measured FROG trace, it is possible to measure it completely with infinite temporal resolution. This is because information from both the time and frequency domain are embedded in the FROG

trace. The range in the time-domain offers long-time resolution of the pulse, while the range in the frequency domain offers short-time resolution.

2.2 Second Harmonic Generation Frequency Resolved Optical Gating

2.2.1 Introduction

The most common of FROG geometries is that of Second Harmonic Generation (SHG) FROG [14, 17]. It has also been referred to sometimes in literature as "spectrally resolved autocorrelation" - as SHG FROG involves spectrally resolving the output of a standard SHG-based autocorrelator. The schematic for SHG FROG is given in figure (1).

The advantage of the SHG FROG geometry is that it is the most sensitive of FROG geometries - since it involves only generating second-order nonlinearity as opposed to higher order nonlinearities. The FROG signal in SHG FROG will therefore be much stronger for a given input signal intensity. Pulses as weak as about 1picoJoule (pJ) energy can be measured with this method.

The drawback with this geometry is that it results in a FROG trace is quite unintuitive. Because the autocorrelation function is symmetric in time, the resulting SHG FROG is also symmetric with respect to delay. This causes an ambiguity in the direction of time for the pulse. That is, a pulse with complex amplitude $E(t)$ will yield the same FROG trace as its time-reversed replica $E^*(-t)$. Although undesirable, this ambiguity is typically removed quite easily by making one additional measurement by distorting the pulse in some known manner - such as adding positive dispersion by inserting a piece of glass into the beam. Only one pulse out of $E(t)$ or $E^*(-t)$ could possibly be consistent with both measurements. The ambiguity is thus resolved.

2.2.2 Improving SHG FROG

Techniques such as FROG have made complete temporal measurement of ultrashort laser pulses measurements - an unsolved problem only a decade ago - not only possible, but also very straightforward. FROG is quite simple to implement compared to other pulse measurement techniques. But as with any technique, there is always an on-going endeavor to

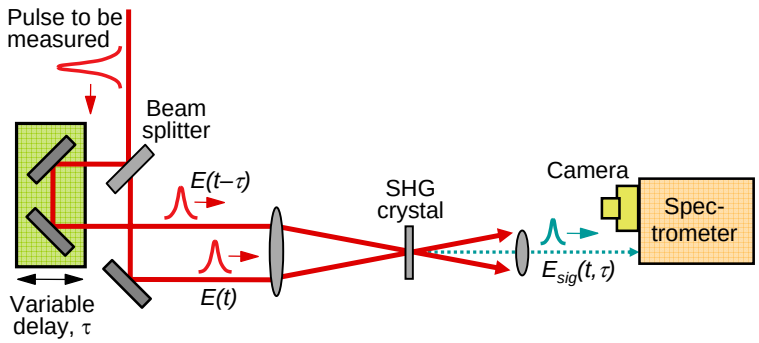

Figure 1: SHG FROG Device Schematic involving an autocorrelator followed by a spectrometer

further simplify its implementation as much as possible. On a practical basis the advantage in doing this is that it would reduce sources for systematic errors in the measurements.

One vital task in building a FROG device is that of calibration of the relevant axes, which is arduous in almost any technique and is always a source for errors. FROG measurements are functions of both delay and frequency. Therefore increments of delay per pixel and wavelength per pixel, respectively, must both be determined during calibration. Mis-calibration of one or both axes can yield high retrieval errors with incorrect results.

Another task in improving SHG FROG is the removal of the ambiguity in the direction of time, that was mentioned in the previous section. While most versions of FROG uniquely determine the pulse, the pulse and its mirror image yield the same trace in SHG FROG, so one must perform additional measurements to determine which pulse field is the true solution. Although FROG contains checks and balances on all measurements, a method for automatic calibration and the removal of this ambiguity would be welcome.

Here, we describe a simple and elegant method proposed and developed by our former postdoctoral fellow, Dr. Erik Zeek, for simultaneously solving both of these problems. Experimental verification of the technique was performed by the candidate. We called this the **Procedure for Objectively Learning the Kalibration And Direction Of Time (POLKADOT) FROG**. POLKADOT FROG can be implemented in a couple of different ways. We discuss various geometries that solve these problems, including one that can be turned on and off with a single knob.

2.3 POLKADOT FROG

Consider the calibration problem first. Its solution was inspired by the FROG trace of a double pulse, as shown in figure (2). The trace contains three islands of intensity, each separated by a pulse separation, τ_{sep}, similar to an autocorrelation of a double pulse which is shown as the delay marginal. In FROG, as opposed to autocorrelation, these islands are frequency resolved. Moreover, in FROG the central island has fringes in frequency with a separation of $1/\tau_{sep}$ as illustrated in the frequency marginal. Thus, the pulse separation determines the spacing of the main structure of the double-pulse FROG trace in both delay and frequency axes.

Thus, by propagating a double pulse with known pulse spacing into a FROG we can automatically extract the increments of both delay and frequency per pixel. This then calibrates the FROG device.

This method works even when the pulse has structure to begin with, provided that the separation of the double pulse is greater than the width of the individual pulses. Accordingly, our solution involves generating a double pulse and identifying these islands and their separation in the resulting trace. This can be done by simply placing an etalon of known optical thickness in the beam path before the FROG device (see figure (3)). Of course, in principle, an etalon produces an infinite train of pulses, but by using an etalon with sufficiently low reflectivity, we can restrict the train to yield essentially one or two additional pulses - all that is needed for calibration.

While the above solution is quite simple, a more elegant solution which came to mind was to replace the usual beam splitter in the FROG device with an etalon (see figure (4)). Here, the etalon's front and back reflectivities must be carefully chosen in order to yield identically shaped pulses in both arms of the FROG device, so that the usual pulse-retrieval algorithm can operate effectively. This is because, the algorithm assumes that the shapes of the two pulses are identical, even though the pulse energies may be different. Specifically, the ratio of the first and second pulse energies in each pulse train should be the same. It is easy to show (Appendix and reference) that this ratio will be the same for both arms as long as the front surface has a 50% reflectivity. Interestingly, the back-surface reflectivity

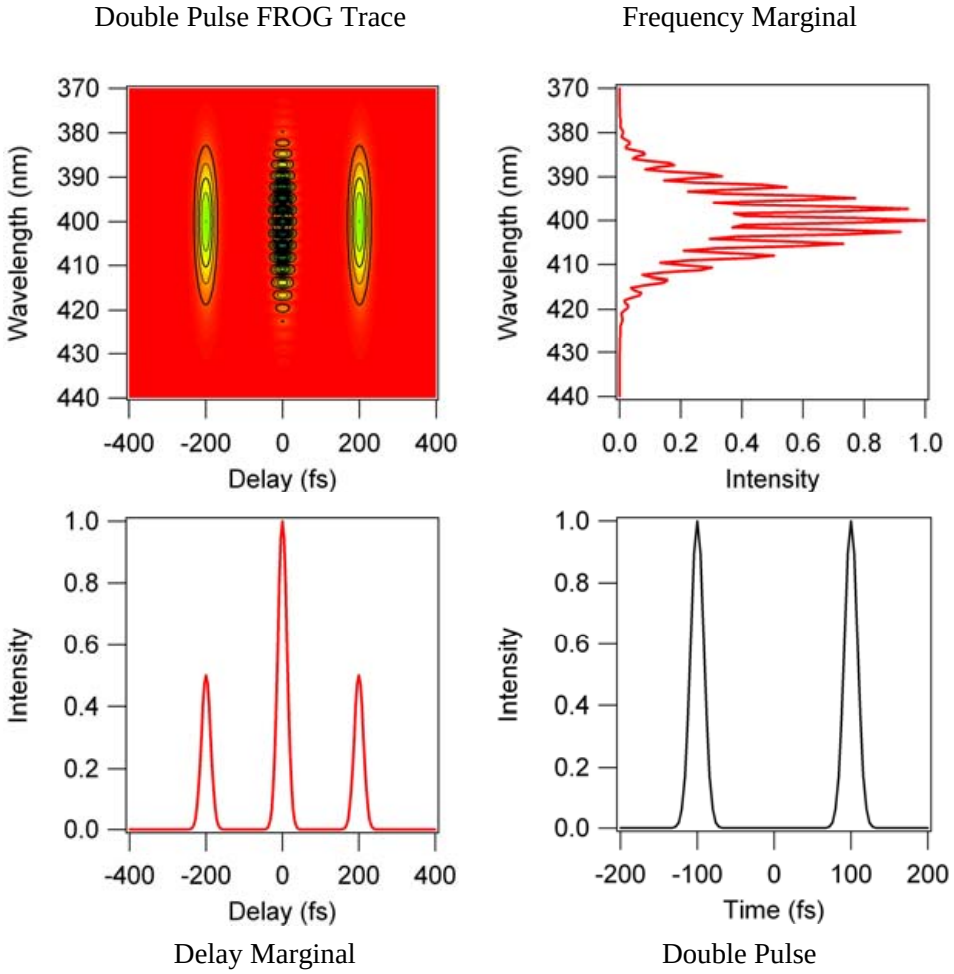

Figure 2: Double Pulse FROG Trace. This figure shows the SHG FROG trace for two 20-fs pulses separated by 200 fs (The pulse train is shown in the lower right-hand corner.). The trace in the upper left shows the square root of the FROG intensity, $\sqrt{I_{FROG}}$. Also shown are the two marginals (integrals of the trace with respect to delay or frequency) that exhibit characteristic modulations.

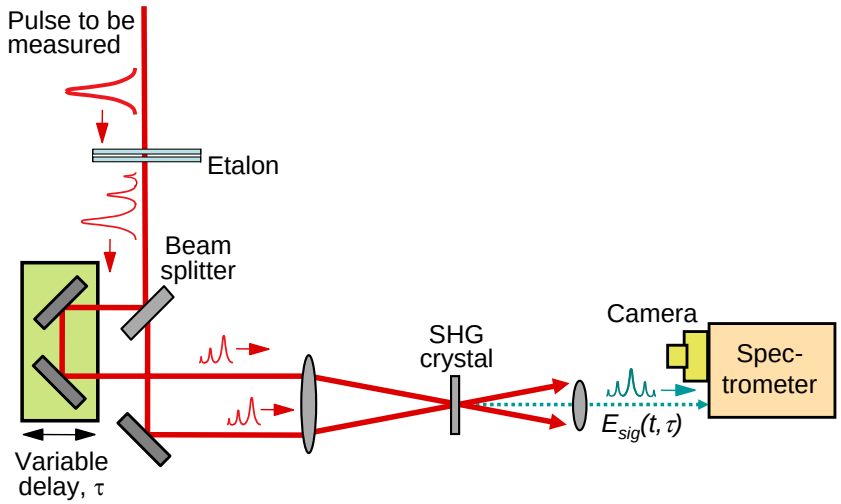

Figure 3: FROG Device Schematic. A schematic layout of an SHG FROG device, showing one of the two possible positions for the etalon in the POLKADOT FROG arrangement, which automatically calibrates the device and removes the ambiguity in the direction of time.

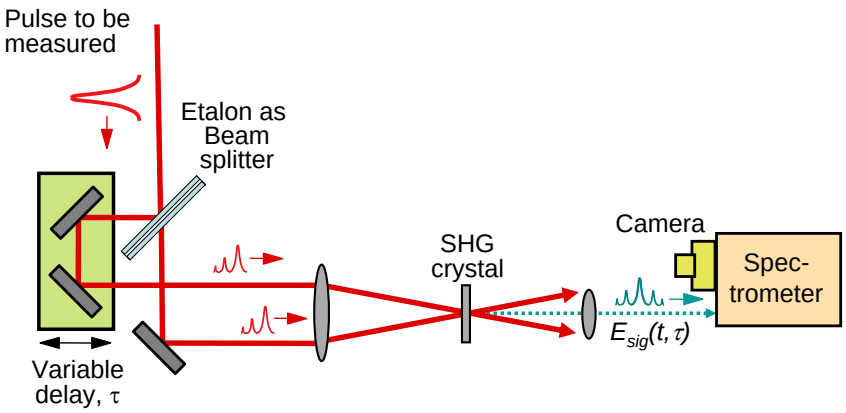

Figure 4: The second, more elegant, schematic layout of an SHG FROG device, showing the etalon as a beam splitter in the POLKADOT FROG arrangement, which automatically calibrates the device and removes the ambiguity in the direction of time.

cancels out of this result and hence can be arbitrary. We chose a value of about 10% for the back-surface reflectivity in our experiments in order to keep the number of additional pulses in the train to a minimum. This also helped minimize the energy wasted in the process of creating such pulse trains. For a back-surface reflectivity of 10%, the second pulse in each arm has 5% of the energy of the initial pulse. Note that, despite the weak intensity of the second pulse, the frequency fringes remain strong: their relative amplitude is given by the geometric mean of the first and second pulse energies, which works out to 45% in the above case.

Finally, for these values of the reflectivities, the third pulse will have an energy that is 0.25% of the first pulse and hence is negligible. (It does introduce slight fringes in the outer islands, which can in fact be used to double check the calibration).

The beam-splitter replacement by the etalon also solves the direction-of-time ambiguity in SHG FROG. The second pulse is necessarily weaker than the first, so it is impossible to confuse the retrieved pulse with its weaker trailing pulse from its mirror image whose weaker pulse leads the stronger one. An etalon has been used to resolve the direction of time ambiguity previously, but POLKADOT FROG marks the use of an etalon as a beam splitter in a pulse measurement device and also the use of an etalon in conjunction with an autocalibration scheme.

POLKADOT FROG requires no change in the FROG pulse-retrieval algorithm. It only requires a somewhat larger scan range (to see the extra islands) and a slightly better spectral resolution (to resolve the spectral fringes). This increase in range/resolution is not significant, as it is not necessary to accurately acquire the details in the wings of the additional islands or in the spectral fringes, but instead only to find their separations.

2.4 Autocalibration using POLKADOT FROG

For the purpose of automatic calibration using the etalon, a simple code was written to find the peaks in the trace. This code does not require the use of the entire FROG trace. Instead, it simply requires computing the frequency and delay marginals. These marginals are, of course, the integrals of the trace with respect to delay and frequency respectively.

The code used a simple peak-finding routine to obtain an initial guess of the peak locations which were then curve-fitted to a sum of Gaussians. The functional form of the equation is:

$$FIT = a + b\tau + c_{back}e^{-((\tau - x_{back})/w_{back})^2} + \sum_{j=0}^{n} c_j e^{-((\tau - x_j)/w_j)^2} \tag{1}$$

where $a+b\tau$ accounts for a flat background with perhaps some slope, c_j is the amplitude of a Gaussian peak, x_j is the center of the peak, and w_j is the width of the peak. Also included is a background Gaussian peak, with the c_{back}, x_{back} and w_{back} parameters. This Gaussian takes into account possible pulse-shape variations and insufficient resolution. This is especially important for the frequency marginal, which has small peaks atop a large peak. The important information in this equation is contained in the x_j parameters. These parameters define the centers of the peaks, and contain the information needed to calibrate the FROG traces. Of course, only once such peak is necessary in each direction, but two or even four or more yield statistical data, which can be fitted for even better results.

Given the peak centers, it was then a simple matter to calculate the calibrations of the FROG trace. The delay spacing $d\tau$ was simply given by

$$d\tau = \frac{\tau_{sep}}{S_\tau}. \tag{2}$$

Here τ_{sep} was the peak-to-peak separation in time and S_τ,the peak-to-peak separation in pixels. The wavelength separation, $d\lambda$ was given by

$$d\lambda = \frac{\lambda_0^2}{\tau_{sep} S_\lambda c}. \tag{3}$$

Here, λ_0 was the center wavelength of the delay marginal, S_λ, the peak separation in wavelength, and c - the vacuum speed of light. The S_λ used in these experiments is the average separation. For very broadband pulses, this is not an exact solution; the separation is constant in frequency, not wavelength. When the bandwidth is small, this effect is not significant. The center wavelength, λ_0, must be determined through an independent method, although halving the fundamental's center wavelength is probably sufficient for most purposes.

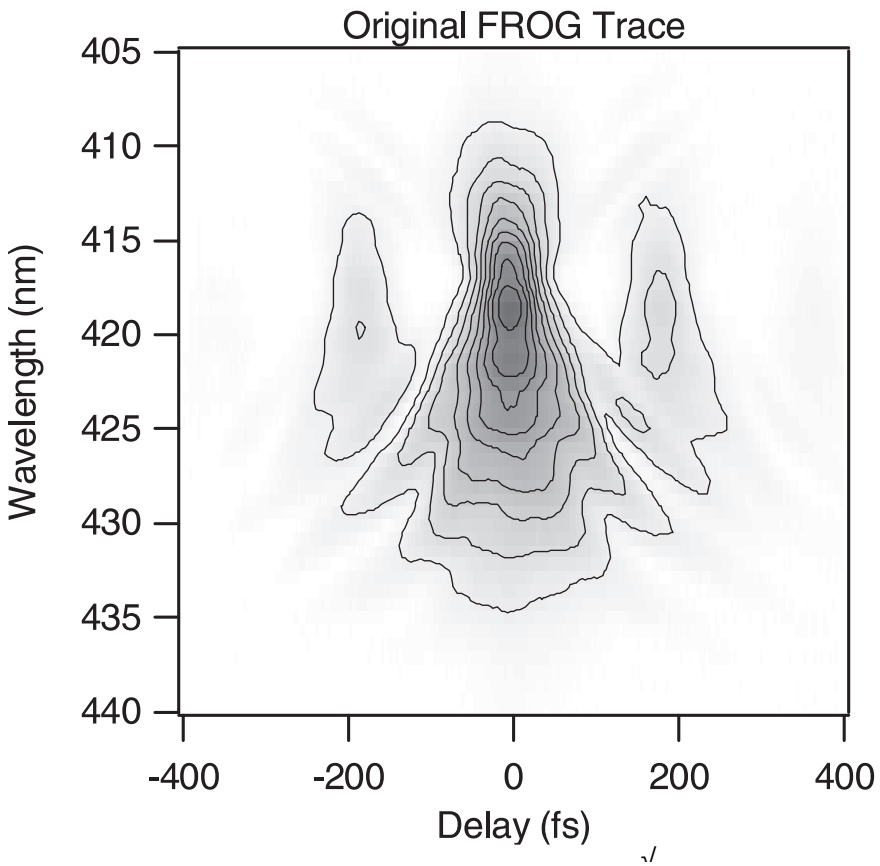

Figure 5: POLKADOT FROG Trace. This is the $\sqrt{I_{FROG}}$ of an SHG FROG trace using a 50%/10% etalon as a beam splitter as described in the text.

We also tested POLKADOT FROG using an SHG FROG device in which we replaced the usual beam splitter with a 26.8-μm etalon having a 50% first surface reflectivity and a 10% second-surface reflectivity, as mentioned. The etalon was air spaced, and the two windows were each 5mm thick. (It is interesting to note that the etalon beam splitter balances the dispersion of both arms. Since the reflective surface is at the center of the beam splitter, all pulses traverse the same amount of glass, and there is no need for a compensation plate in either arm.) This etalon yielded pulses separated by 179 fs. The etalon spacing was itself easily calibrated by measuring the spectrum of light transmitted through it and using the same formula as above for the fringe spacing. To measure this, we used a commercial spectrophotometer, a Varian Cary 500 Scan, and fit the peaks using a simple LabVIEW code.

The SHG FROG device in these experiments used a 100-μm thick KDP crystal and a beam angle of 5°. The delay was stepped using a Newport MFN25PP translation stage and ESP 300 controller. The spectrometer was an Acton Research Spectra Pro 150 with a 1200 gr/mm grating. An Oriel Instaspec II pda camera was used to acquire the spectra.

We deliberately used a somewhat distorted pulse whose FROG trace obtained using POLKADOT FROG is shown in figure (5) which clearly shows one pair of additional islands. The marginals for the FROG trace are shown in figure (6) (the delay marginal) and figure (7) (the frequency marginal). Fitting Eq. (1) to each set of marginals, we determined the peak locations, as shown in figure (8). The fitting was performed by Matlab code developed for this purpose. For both marginals, we were able to obtain more than one set of additional peaks. Using a simple linear fit, we determined the average spacing between the peaks. For the delay marginal, the spacing was 51.6$\pm$0.2 pixels and for the frequency marginal, the spacing was 28.9$\pm$0.5 pixels. This yielded a temporal calibration of 3.47$\pm$0.01 fs/pixel and a frequency calibration of 0.106$\pm$0.002 nm/pixel, using 405 nm as the center wavelength. Both axes were also calibrated through more traditional means. The delay calibration was read directly from the encoder on the translation stage. The step size was 0.518 μm, which yields a temporal spacing of 3.46 fs/pixel. The spectrometer was calibrated using a Kr-vapor lamp. By fitting several spectral lines, the spacing was found to be 0.1067 fs/pixel.

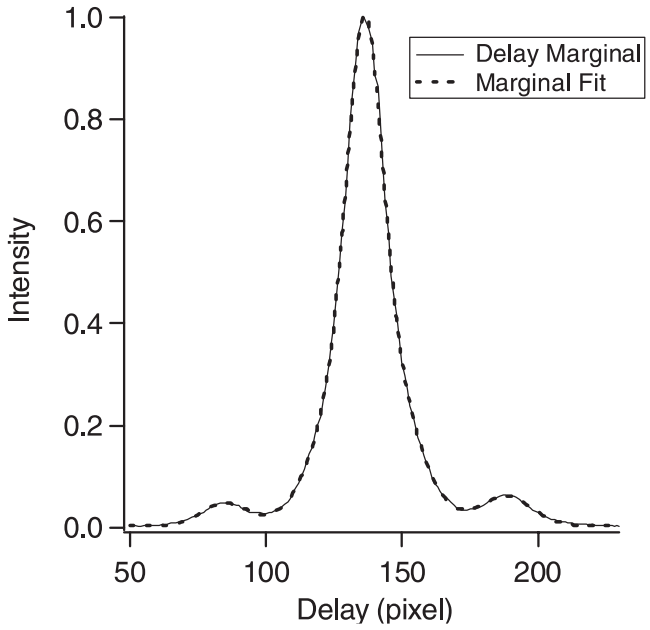

Figure 6: Delay Marginal (equal to the pulse intensity autocorrelation). The delay marginal has peaks separated by the pulse separation. The fit of Function (1) to the marginal is also shown.

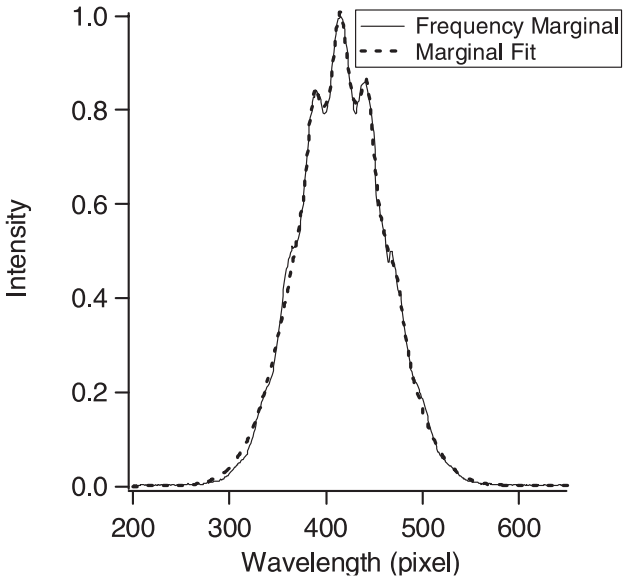

Figure 7: Frequency Marginal (equal to the autoconvolution of the spectrum). The frequency marginal has peaks separated by the reciprocal of the pulse separation. The fit of Function (1) to the marginal is also shown.

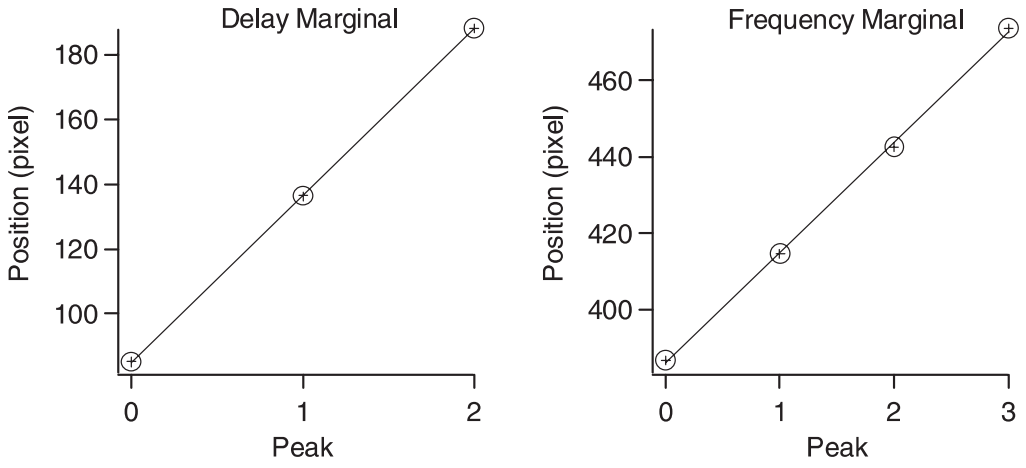

Figure 8: Peak Positions and Calibration Fit Functions. Shown here are the peak positions from the marginals and the straight line fits. The delay marginal fit was 84+951x, and the frequency marginal fit was 38+628x, where x is the peak number.

The etalon calibration values were easily within experimental error of the independently determined values.

We have also simulated the performance of this device on a complex pulse, in particular, a pulse with a Gaussian spectrum and spectral quadratic and cubic phase, shown in figure (2.4). In this case, the pulse had structure that could, in principle, confuse the fitting procedure. However, the FROG trace and the resulting marginals smoothed out this structure, leaving only the desired structure. In addition, it must be admitted that pathological cases in which the pulse is in fact a double pulse separated by approximately the etalon round-trip time can confuse this procedure. One is cautioned not to use such pathological pulses in the calibration stage!

Overall, we found this approach to calibration quite satisfying. It is more reliable for the delay calibration than the use of a commercial translation-stage calibration, which is subject to mechanical problems that can be difficult to track down. In one of our trials, a translation stage exhibited different calibrations in different regions of its travel. Thus, a calibration obtained in one region would not have been valid in the other. POLKADOT FROG solves this problem elegantly, and, even better, it involves no moving parts (although there may be moving parts in the FROG device itself), and it continually recalibrates the device for every

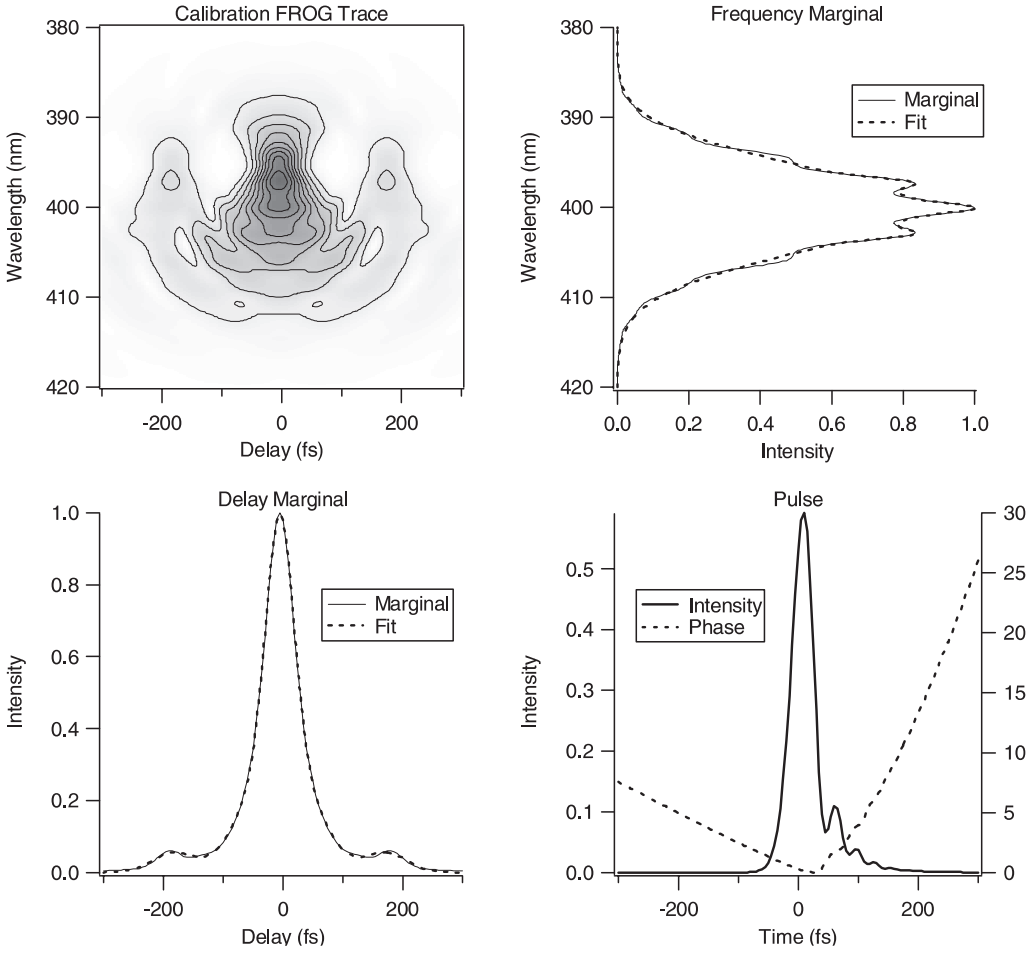

Figure 9: A complicated theoretically reconstructed POLKADOT FROG Trace. The trace in the *upper left* was created from the pulse in the *lower right*, assuming that the pulse had passed through a 50%/10% etalon that created a pulse separation of 180 fs. Again, the $sqrtI_{FROG}$ is shown in the *upper left*. The original trace had a time calibration of 5000 fs/pixel and a spectral calibration of 0.1043 nm/pixel. The retrieved calibrations were 5067 fs/pixel and 0.1065 nm/pixel.

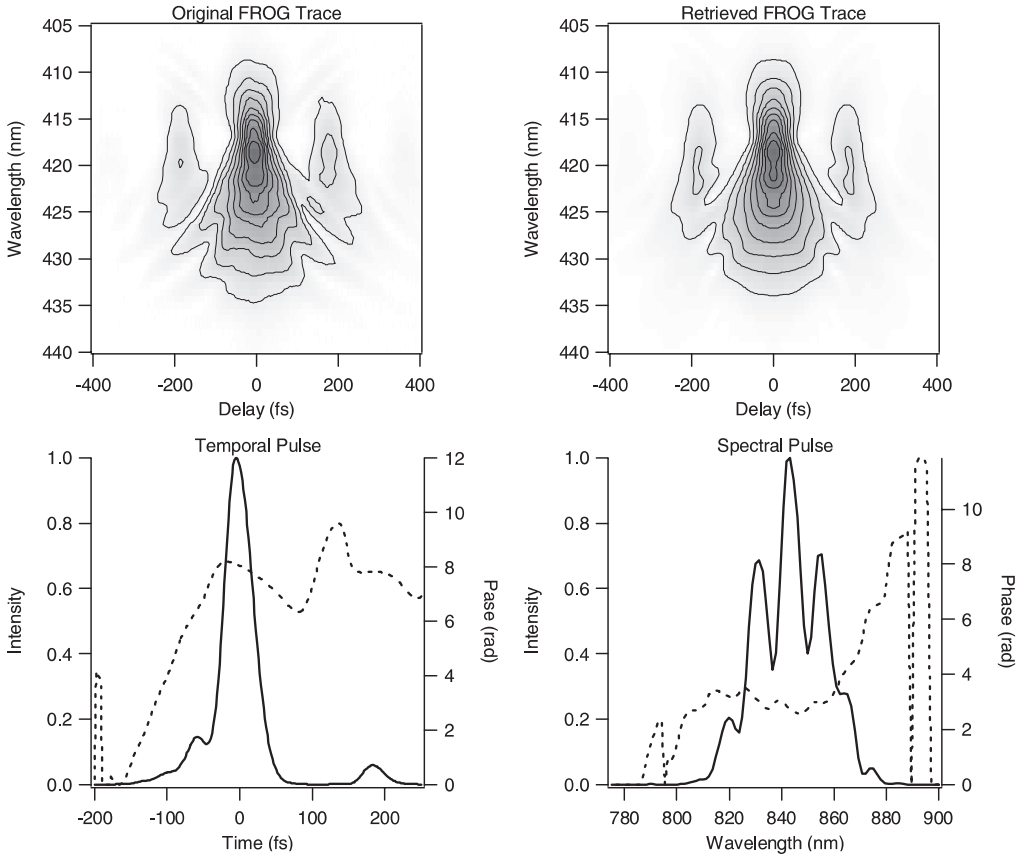

Figure 10: Retrieved POLKADOT FROG Trace (*top right*) and retrieved pulse (*bottom*). This retrieval clearly shows the secondary pulse, indicating the direction of time.

measurement. The POLKADOT option can be used in all FROG variations. In addition, it is easy to imagine many other methods for fitting the peaks. For example, one could force the peaks to be equally spaced, thus allowing only one peak separation parameter. Alternatively, one could also incorporate a multiple-pulse formula into the FROG algorithm.

2.5 Removal of the Direction-of-Time Ambiguity with POLKADOT FROG

In addition to calibrating the trace, POLKADOT FROG removes the direction-of-time ambiguity from an SHG FROG trace. Figure (10) shows the pulse retrieved from the SHG FROG trace in figure (5). Ordinarily, the retrieved pulse in an SHG FROG measurement would be ambiguous because the pulse obtained by the algorithm and its mirror image in time would yield the same measured FROG trace and so it is not possible to determine

which is correct. However, in our case, having used an etalon, we know that the second pulse is much weaker than the first, and we also know when it occurs. In the pulse shown in figure (10), the secondary pulse must occur at about +180 fs. This is clearly evident in the temporal pulse retrieved and hence is easily identified as the second pulse in the train. Thus, the POLKADOT FROG geometry also eliminates the direction-of-time ambiguity in SHG FROG.

Of course, when we measure a pulse, we wish to obtain that pulse, not a version of it with a weak second pulse trailing behind it. Fortunately, the removal of the second pulse is straightforward. Note that, more precisely, an infinite train of additional pulses follows behind the first pulse, each delayed by τ and reduced by a factor of, say, ε. Thus POLKADOT FROG yields a measured field, $E_{meas}(t)$, with additional delayed replicas of the pulse field:

$$E_{meas}(t) \;=\; E(t) + \varepsilon\, E(t-\tau) + \varepsilon^2\, E(t-2\tau) + ... \tag{4}$$

where $E(t)$ is the actual pulse, which we desire. To obtain $E(t)$, it is simply necessary to subtract off the measured field reduced in magnitude by ε and displaced by τ : that is, by subtracting off the quantity: $\varepsilon E_{meas}(t-\tau)$. This yields a new quantity:

$$E'_{meas}(t) \;=\; E_{meas}(t) - \varepsilon\, E_{meas}(t-\tau) \tag{5}$$

.

Substitution of $E_meas(t)$ into this expression, followed by some simple arithmetic yields:

$$E'_{meas}(t) \;=\; E(t) \tag{6}$$

.

Thus, it is trivial to obtain $E(t)$ from the measured field. The pulse shown in figure (11) is the same as the pulse from figure (10) with this simple correction procedure applied and shows remarkably good removal of the secondary pulse. A more convenient algorithm could be developed as part of the FROG retrieval. By including the multiple pulse nature

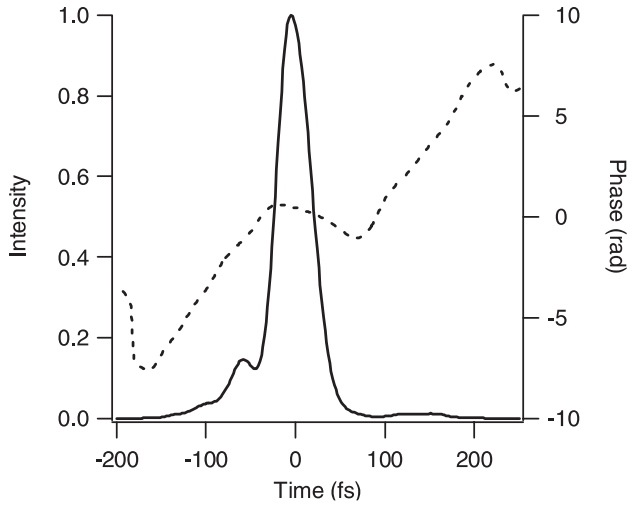

Figure 11: The Corrected POLKADOT FROG Retrieved Pulse. The pulse after subtracting off the trailing pulses as described in equation (5). The secondary pulse is completely gone.

of the FROG trace inside of the algorithm, $E(t)$ could be retrieved directly from the trace.

Interestingly, it is possible to set up a version of this technique in which one can simply convert from standard FROG to POLKADOT FROG. It involves using an etalon at Brewster's angle with no coating on the second surface. As a result, the back surface will have a reflectivity of about 10% for the s-polarization and 0% for the p-polarization. The etalon should at the same time be designed to have a 50% reflectivity for the s-polarization, and any reflectivity between about 25% and 75% for the p-polarization. As a result, an input pulse with s-polarization will be transformed to a train of pulses and will experience the POLKADOT effect, while a pulse with p-polarization will not see the POLKADOT effect and will participate in a standard FROG measurement. Since it is very easy to rotate the polarization of a pulse before the FROG device (using a half-wave plate), this POLKADOT FROG arrangement could be very convenient.

Finally, a minor practical issue: of course, the relatively thick (off-the-shelf) optical elements of the etalon used in this work distorted our pulse and would seriously distort extremely short pulses. Obviously, the thinner the elements used, the less distortion will be present. For extremely short pulses, one could use an ultra-thin piece of glass as the etalon.

To conclude, in this chapter, we discuss a simple variation of the FROG technique that

we developed called POLKADOT FROG. This technique automatically calibrates the device in both delay and frequency and simultaneously removes the ambiguity in the direction of time in SHG FROG. It is simple to implement, requiring only the replacement of the beam splitter with an etalon. In alternative versions of FROG, such as GRENOUILLE [31], where no beam splitter is used, the etalon is placed in front of the device and removed when no longer needed. Most versions of FROG should benefit from this simple addition.

CHAPTER 3

SPECTRAL INTERFEROMETRY

3.1 Introduction

FROG and its more elegant avatar GRENOUILLE can measure ultrashort pulses which have pulse energies in the pJ regime and perhaps even in the 100s of fJ. But many experiments result in the generation of ultrashort pulses that are much weaker. The drawback in using FROG and any typical pulse measurement technique is the reliance on nonlinear-optical processes [43, 44], which make measuring weak pulses difficult, if not downright impossible.

Fortunately there is a *linear* technique that is available to measure the intensity and phase of such weak pulses with great sensitivity, as long as there is a fairly intense pulse available which has similar or broader, overlapping spectral bandwidth. This technique is called **Spectral Interferometry (SI)**. SI, as the name suggests, involves measuring the interference spectrum from the sum of the two pulses. From the resulting interference fringes, the spectral phase difference $\Delta\varphi(\omega) = \varphi_{strong}(\omega) - \varphi_{weak}(\omega)$ between the strong pulse and the weak pulse can be measured. If the phase of the stronger pulse is known (having been measured previously using, say, a FROG technique), then the phase of the weak pulse $\varphi_{weak}(\omega)$ can be extracted easily. The main advantage of this linear technique is that it is a so-called *heterodyne* technique, as the weak pulse is not measured directly; it is summed with a stronger pulse, making it more visible and easier to measure. An additional advantage of SI is that it does not involve iterative algorithms to measure the phase.

The combination of using FROG to measure the "reference" pulse and SI to then measure the weaker "unknown" pulse has been called *Temporal Analysis by Dispersing a Pair of Light E-fields* or TADPOLE for short. TADPOLE has been shown to measure pulse trains with individual pulses having 42 zeptoJoules (zJ) of energy [19].

Fourier Transform Spectral Interferometry (FTSI) was first introduced by Froehly et. al [20, 32]. The signal whose E-field is given by $E_{unk}(t)$ and the reference pulse, $E_{ref}(t)$

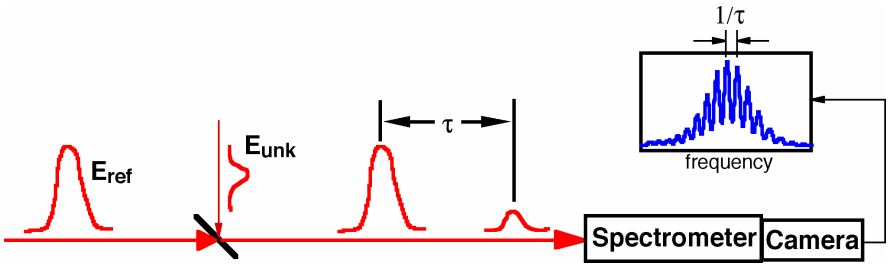

Figure 12: Simple schematic for Spectral Interferometry experiments. The unknown and reference pulse are interfered collinearly and the spectrum resolved in a spectrometer.

are directed collinearly into a spectrometer with a delay τ between them. As long as the spectrum of the reference pulse encompasses the spectrum of the signal pulse, there will be spectral interference between the two pulses. The resulting SI spectrum is then given by:

$$S_{SI}(\omega) = S_{ref}(\omega) + S_{unk}(\omega) + 2\sqrt{S_{ref}(\omega)}\sqrt{S_{unk}(\omega)}\cos[\varphi_{unk}(\omega) - \varphi_{ref}(\omega) - \omega\tau]. \quad (7)$$

Here, $S_{ref}(\omega)$ and $S_{unk}(\omega)$ refer to the spectra of the reference and signal pulses respectively. Since the phase of the reference is known, a simple inversion algorithm can be used to extract the phase of the signal pulse.

The most common inversion technique called FTSI or alternately, frequency-domain interferometry, involves a one-dimensional Fourier transform, which makes the retrieval much faster than FROG algorithms, especially for complicated pulses. Here, the relative delay between the two pulses τ emerges automatically from the analysis and does not have to be measured independently.

Dual-Quadrature Spectral Interferometry (DQSI) [27, 19] is an alternate to FTSI. Here along with measuring the usual SI signal, an additional measurement is made by inserting a $\pi/2$ phase shift in one arm of the interferometer, so that the new interference spectrum now becomes:

$$S_{SI}(\omega) = S_{ref}(\omega) + S_{unk}(\omega) + 2\sqrt{S_{ref}(\omega)}\sqrt{S_{unk}(\omega)}\sin[\varphi_{unk}(\omega) - \varphi_{ref}(\omega) - \omega\tau]. \quad (8)$$

.

This allows for the non-interferometric parts of the signals to be removed leaving only the sine and cosine parts of the signal. By setting the delay $\tau = 0$, it is possible to determine the phase difference $\Delta\varphi(\omega) = \varphi_{ref}(\omega) - \varphi_{unk}(\omega)$ uniquely, thereby allowing φ_{unk} to be extracted. This is a very elegant way to measure the phase. Although used in time domain, this technique has not been demonstrated to measure spectral phase until now.

Other SI techniques involve phase-shifting over $0°, 90°, 180°$ and $270°$ and making multiple spectral measurements. There are several variations of such phase-shifting SI depending on the number of spectra measured, all intended to measure phase. Typically such phase-shifting interferometric techniques are applied to measure phase in spatial domain.

3.2 SI to measure picosecond-long shaped pulses

3.2.1 Practical limitations of SI

It is often possible to shape ultrashort laser pulses into potentially complex waveforms with time-varying intensity and phase. In such instances, iterative algorithms become too slow to be able to process complex pulses generated by such pulse-shapers effectively. The pulse-shapers require rapid feedback from the measurement to the shaper to verify that the pulse shape is correct. These applications typically involve varying a shaped pulse and seeing what happens to a sample medium excited by the pulse, and then trying another pulse shape. In such applications, speed is very critical. SI, with its direct inversion algorithm, offers a perfect solution to such problems.

SI overcomes the requirement for spectral overlap with the shaped pulse because the shaped pulse is always obtained from an initial input pulse, which can be treated as a reference pulse.

Although spectral interferometry has many advantages, its application is often limited due to a serious practical difficulty: to obtain clear interferometric "fringes", the object beam and the reference beam must be aligned perfectly collinearly, down to a few microradians, which involves four very sensitive alignment degrees of freedom. This is time-consuming to achieve and often difficult to maintain during the course of the experiment, as the beam walks during alignment. In addition, significant attenuation is also required in SI

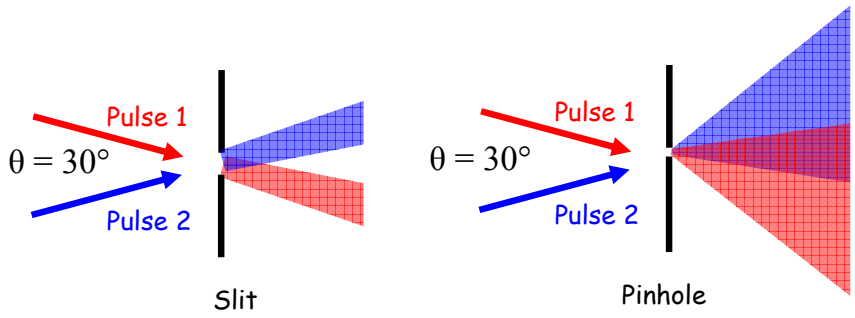

Figure 13: Schematic representing the advantage of replacing a spectrometer slit with a pinhole.

measurements because the technique is so sensitive, and the required neutral density or other filters can distort the pulse. Finally, because pulse-shaping often involves lengthening the pulse significantly, to nearly 10 picoseconds in some cases, the required spectral resolution can be quite high - much higher than that required to measure the original pulse. As a result, SI is rarely used to measure shaped pulses. But, if we can solve these problems, SI could become the standard method for measuring shaped pulses.

The collinear alignment requirement comes from the fact that the two pulses need to remain overlapped spatially in order to interfere at the entrance slit of the spectrometer. However, if a pinhole (or a very tiny slit) of the order of the wavelength of the pulses is used at the entrance of the spectrometer in the place of the usual slit, we find that it relaxes the stringent constraint of collinear alignment. This is a simple improvement that we present to spectral interferometry, which significantly reduces the alignment requirement of the technique. This is because the two beams entering the pinhole will diffract at the pinhole and "forget" their original direction. Now, even if the two beams enter the pinhole at large crossing angles, they would still maintain spatial overlap thus requiring only the temporal delay τ to be defined to produce fringes. As a bonus, the pinhole achieves significant attenuation making away with the need to use neutral density filters in the measurement. And an added advantage is that the spectral resolution of the spectrometer is optimal with such a small entrance pinhole.

3.2.2 Experiment

We tested the pinhole idea by modifying a 250-cm-optical-length Oriel Instruments MS257 spectrometer. The entrance slit assembly was replaced by a $\sim 14\mu m$ diameter pinhole, which we made on a stainless steel sheet by focusing amplified Ti:sapphire pulse onto it. The size of the pinhole was determined by measuring the Airy rings. We used the output from a KM Labs Ti:sapphire oscillator as the reference pulse, and measured its intensity and phase using a Swamp Optics GRENOUILLE. In this preliminary work, the object pulse consisted of a double pulse from a Michelson interferometer. A beam-splitter was used in the reference arm to provide the input to the Michelson interferometer. Its spectrum had fairly broad fringes due to the interference of the two pulses. The object double pulse and the reference pulse were both sent into the spectrometer through the small pinhole, at a large crossing angle of nearly 32°, mutually delayed. The delay between the object pulse and the reference pulse was adjusted to produce the fine fringes that our spectrometer was able to resolve, because a smaller fringe spacing allowed for smaller features in the object pulse spectrum to be retrieved reliably by SI. We measured the SI spectrum with a spectrometer and a photodiode array, and ran the FTSI inversion TADPOLE algorithm to obtain the intensity and phase of the object pulse both in the time and frequency domains.

Since the double pulse was generated by using replicas of the reference pulse which had been previously characterized, we expected each peak of the double-pulse to be identical to the reference pulse, but separated by the delay corresponding to the delay measured from the fringes in the double-pulse spectrum. As can be seen from figures (14,15), the TADPOLE algorithm retrieved the two pulses forming the double-pulse in time very accurately. The limitation in the Oriel spectrometer resolution of 0.35 nm limited our ability to measure long double pulses, the longest pulse we could measure being ~ 3 ps.

We replaced the Oriel spectrometer with an Ocean Optics HR4000 fiber spectrometer which had a spectral resolution of 0.05 nm. With this spectrometer, we were easily able to measure broadband double pulses separated by as much as 10 ps, as shown in figure(16). The algorithm does an excellent job of retrieving the phase of the pulse. The intensities of the two peaks in the double pulse are of different heights due to the fact that we have

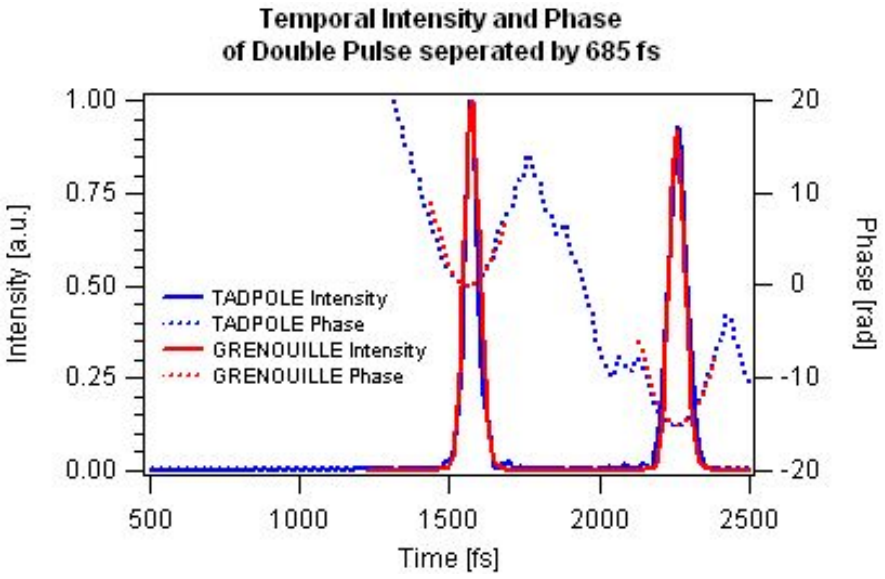

Figure 14: The intensity and phase of a TADPOLE retrieval of a 685 fs long double-pulse is shown in the time domain. The intensity of the GRENOUILLE measured reference pulse is superimposed on this retrieval and shows excellent agreement.

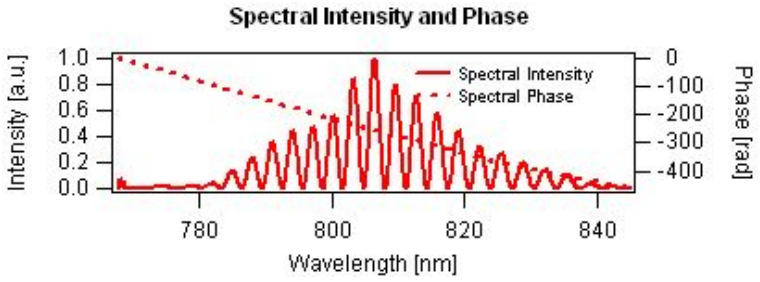

Figure 15: The spectral intensity and phase of a TADPOLE retrieval of a 685 fs long double-pulse is shown in the time domain.

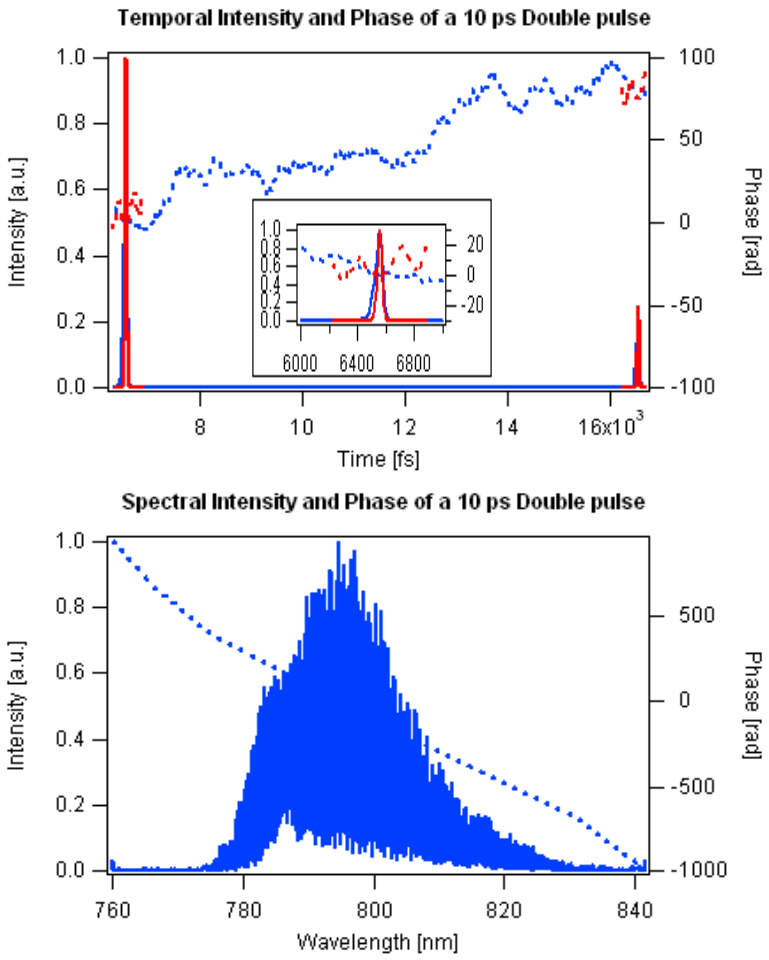

Figure 16: The intensity and phase of a TADPOLE retrieval of a 10 ps long broadband double-pulse is shown in both the time and spectral domain. The inset in time domain shows the first peak of the double pulse clearly.

fine fringe spacing which results in poor fringe visibility [15, 16]. Although we tried to characterize the apparatus function to account for this poor visibility, we were unsuccessful in deconvolving the apparatus function accurately in our data. That also accounts for the less than perfect spectral retrieval.

The idea of using pinholes to make alignment-free SI set-ups can be improved even further by use of single-mode optical fibers whose cores act as pinholes, essentially the same idea. Only the component of light which mode-matches the fiber will couple into it. Again attenuation is provided automatically, because of the small core size.

3.3 Background-free Spectral Interferometry and Practical devices for SI

3.3.1 Differential Spectral Interferometry

In the previous section, we suggested replacing the slit with a pinhole as a simple way to overcome the experimental hindrance to SI which would make it a more prevalent technique for pulse measurements in laboratories. There is however another drawback to SI which makes processing the data obtained from SI experiments difficult. There is always a strong (DC) background associated with the light source itself that is inherently present in all SI images. The experimental outcome of this DC term is that the pulses in SI measurements are deliberately not overlapped in time, but kept at fairly large delays in order to yield distinct spectral fringes far away from DC in the SI spectrum that the Fourier transform based inversion algorithm can isolate and retrieve accurately. This forces the spectral resolution of the spectrometer to be as much as 10 times longer than the pulse length itself, simply to measure the pulse spectrum. When measuring shaped pulses that run up to 10 ps in length, this feature of SI could be undesirable as it would mean very large and *very expensive* spectrometers. It would be a great advantage for the technique to be able to eliminate such strong DC background and be able to overlap the pulses in time in spectral interferometry to measure long complex pulses.

A new method of SI called Differential Spectral Interferometry (DSI) was introduced a couple of years ago that gets around the background problem in a very simple manner [41]. DSI involves introducing a π phase shift in one arm of the interferometer and making an additional interferometric measurement. A differential spectral interferogram is then obtained by subtracting one spectrum from the other, thus eliminating the DC terms and increasing the signal of interest by a factor of 2 compared to the SI.

$$\begin{aligned} S_{SI}^{+}(\omega) &= |E_{ref}(\omega)|^2 + |E_{unk}(\omega)|^2 + E_{ref}(\omega) E_{unk}(\omega) \cos[\varphi_{ref}(\omega) - \varphi_{unk}(\omega) - \omega\tau] \\ S_{SI}^{-}(\omega) &= |E_{ref}(\omega)|^2 + |E_{unk}(\omega)|^2 - E_{ref}(\omega) E_{unk}(\omega) \cos[\varphi_{ref}(\omega) - \varphi_{unk}(\omega) - \omega\tau] \end{aligned} \tag{9}$$

so that,

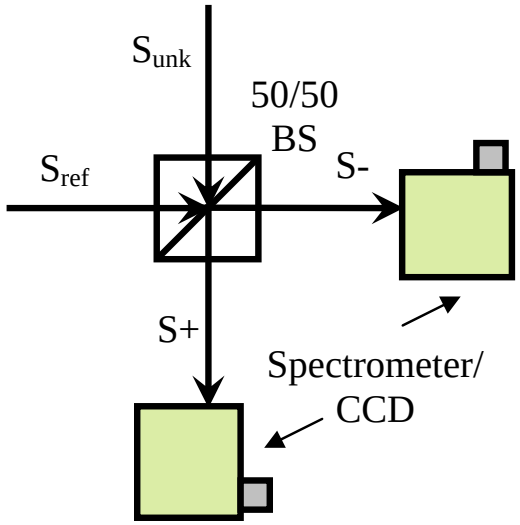

Figure 17: Differential Spectral Interferometry schematic.

$$S_{SI}^{+}(\omega) - S_{SI}^{-}(\omega) = 2\, E_{ref}(\omega)\, E_{unk}(\omega) \cos\left[\varphi_{ref}(\omega) - \varphi_{unk}(\omega) - \omega\tau\right] \tag{10}$$

.

Experimentally the idea is very simple to implement, since a 50/50 beam-splitter provides a π phase shift with the proper intensities to eliminate DC terms. However the alignment requirement in this case is more stringent than that of spectral interferometry.

Taking the fiber-coupling idea, that we introduced in the last section further, a very

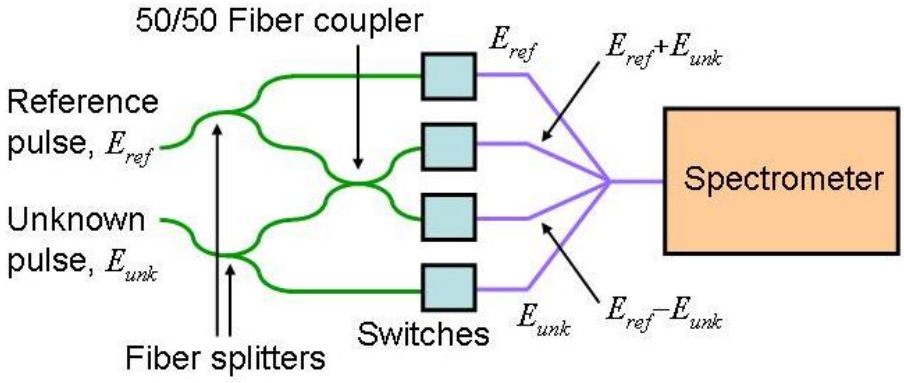

Figure 18: Fiber Coupled Differential Spectral Interferometry schematic.

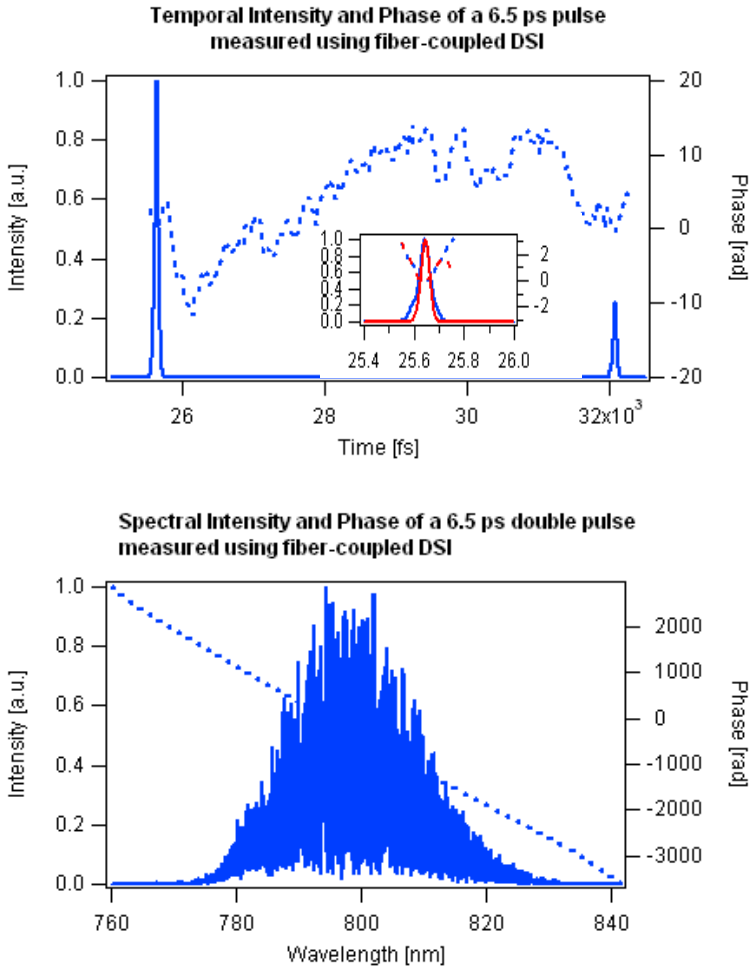

Figure 19: The intensity and phase of a TADPOLE retrieval of a 6.5 ps long broadband double-pulse is shown in both the time and spectral domain. The experiment was performed using an elegant fiber-coupled Differential Spectral Interferometric scheme. The inset in time domain shows the first peak of the double pulse clearly. There is very little background present in such a scheme.

elegant differential spectral interferometric scheme can be implemented with the use of fiber couplers, as shown in figure (18), which is easy to align and maintain alignment.

The fiber splitters in the 1×2 couplers split off pieces of the two input pulses, so that their spectra may be measured separately. The 2×2 fiber coupler (which acts as a 50/50 beam splitter) yields two outputs which are the sum and difference of the two input pulse fields [9]. The switches shown in the schematic then allow one of the four outputs to enter the spectrometer at any given time, rapidly scanning all four outputs. As long as the fiber lengths in the two interferometric channels are kept identical, the contributions of Group Velocity Dispersion (GVD) in the various fibers of this device cancel out and the pulse is retrieved accurately.

We have performed preliminary measurements with such a practical device and we have found that pulses with very large separations can be measured by using the full spectral resolution of the spectrometer using the DSI scheme, without a large DC background to worry about. Shown in figure (19) is one such measurement of a 6.5 ps long double pulse. There is good agreement between this TADPOLE retrieval and the GRENOUILLE measurement of such a pulse, especially in the phase retrieval.

Although in principle DSI should work exceeding well, in practice this only occurs when the two fibers being used for the two interferometric measurements are exactly identical. It is exceedingly difficult to manufacture the two fibers in the fiber coupler to be exactly identical. Shown in figure (20) is the variation of the response with wavelength of the two arms of the 2×2 fiber-coupler that we used in our experiment. What this implies is that although there is only a π-phase shift between the two measurements S_+ and S_-, it is never possible to cancel out the DC background completely.

In addition, the TADPOLE algorithm that we have used to retrieve all these pulses use Fourier transform inversion. However with ease of alignment and ability to automate data gathering, it is tempting to implement alternate schemes for inversion such as Dual Quadrature Spectral Interferometry or Phase Shifting Interferometry.

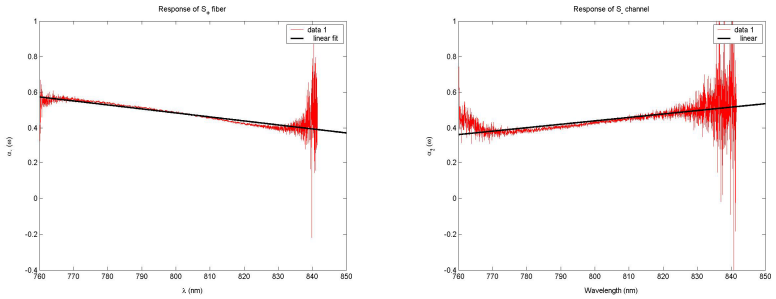

Figure 20: The two arms of a 2×2 fiber coupler are not identical in their response at different wavelengths. This implies that the SI spectra measured on the S_+ and S_- channels of the coupler will not cancel out in DC completely.

3.3.2 Dual-Quadrature Spectral Interferometry

Dual-Quadrature Spectral Interferometry (DQSI) furthers the idea of measuring two SI spectra to retrieve the phase of the unknown pulse. Only this time, in the second measurement, instead of shifting the phase between the two arms of the interferometer by π, we introduce a $\pi/2$ phase-shift between the two arms. Experimentally this can be done by simply introducing a quarter-wave-plate in the reference arm or increasing the delay between the reference arm and the object pulse arm. In our case, we allowed the slow-drift in the spectrum due to the fiber to furnish us with the required $\pi/2$ phase-shift. This has the consequence that the SI equations now change to

$$\begin{aligned} S_{SI}^{R}(\omega) &= |E_{ref}(\omega)|^2 + |E_{unk}(\omega)|^2 + E_{ref}(\omega) E_{unk}(\omega) \cos[\varphi_{ref}(\omega) - \varphi_{unk}(\omega) - \omega\tau] \\ S_{SI}^{I}(\omega) &= |E_{ref}(\omega)|^2 + |E_{unk}(\omega)|^2 + E_{ref}(\omega) E_{unk}(\omega) \sin[\varphi_{ref}(\omega) - \varphi_{unk}(\omega) - \omega\tau] \end{aligned} \tag{11}$$

,

so that we can now simple add the two measurements in the following form:

$$S_{SI} = S_{SI}^{R} + i\, S_{SI}^{I} \tag{12}$$

yielding a complex number, whose phase is simple the phase we are after. This inversion routine is exceedingly simple requiring no Fourier transforms to extract the spectral phase. Subtracting the linear term from the phase- due to delay τ, and the phase from due to the

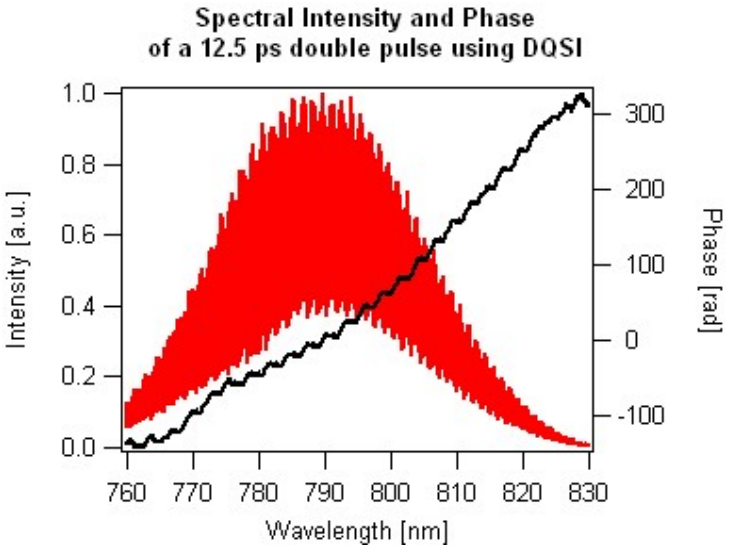

Figure 21: The spectrum and spectral phase of a TADPOLE retrieval of a 12.5 ps long broadband double-pulse. The experiment was performed using a fiber-coupled Dual-Quadrature Spectral Interferometric scheme.

reference pulse, we have the phase of the unknown pulse we are after quite simply. At this point, if necessary, a Fourier transform would allow us to get the intensity and phase of the pulse in the time domain.

Other than ease of inversion algorithm to extract phase, this technique is also powerful in that it allows the full spectral resolution of the spectrometer to be utilized, or alternately, in the time domain, access the entire range in the time domain that is available. This is because we no longer have to worry about the signal in the negative delay axis being a reflection of the signal from positive delay. The signal that we see in the time domain is entirely due the pulse we have been trying to measure.

This technique thus provides a very neat, elegant and powerful method of applying Spectral Interferometry to measure long shaped pulses.

As an aside, the phase jumps in the measurement of our pulse in the spectral domain are real and occur due to the fact that the two peaks are of comparable intensities. This can be seen from the following calculations:

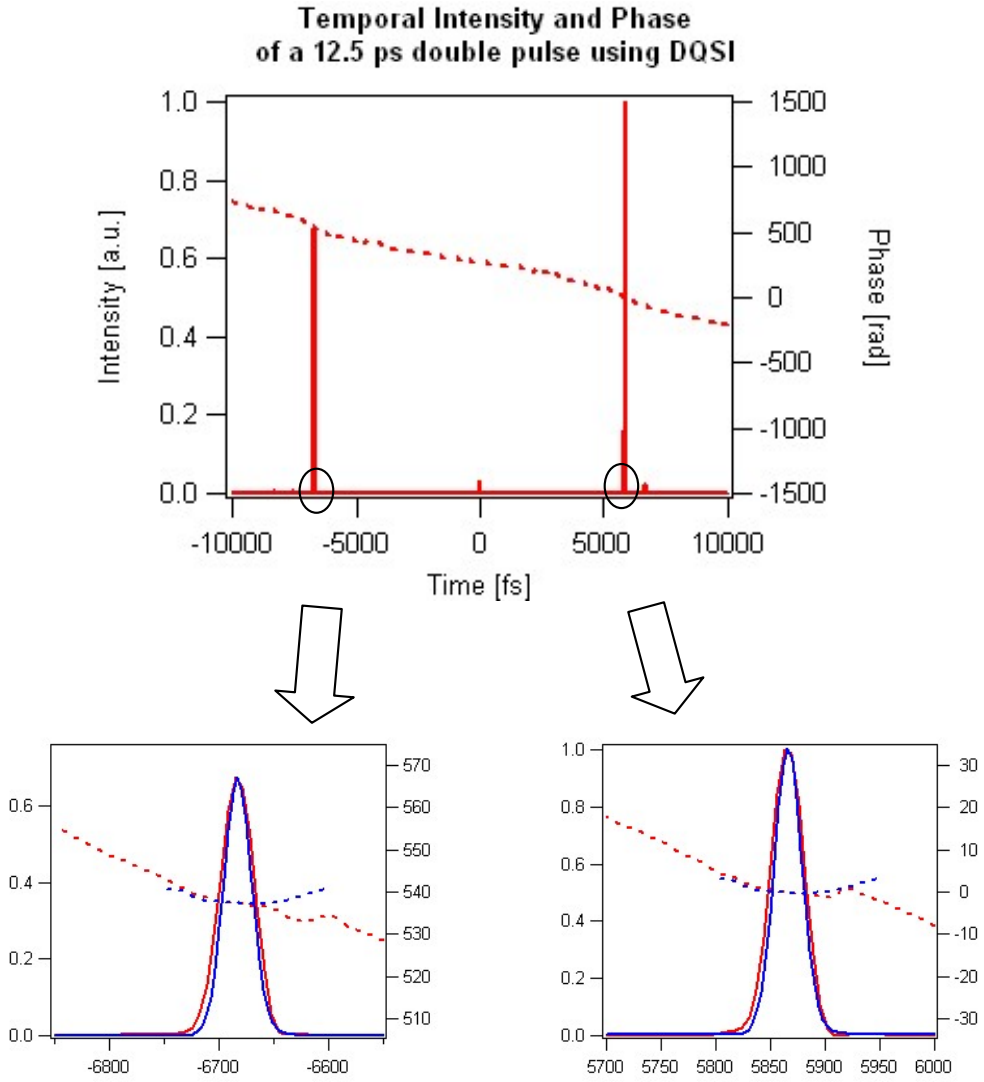

Figure 22: The intensity and phase of a TADPOLE retrieval of a 12.5 ps long broadband double-pulse is shown in time domain. The experiment was performed using a fiber-coupled Dual-Quadrature Spectral Interferometric scheme. The expanded figures at the bottom show the each peak of the double pulse clearly, compared with the GRENOUILLE measured reference pulse. There is excellent agreement between the GRENOUILLE measurement and the TADPOLE retrievals. There is very little background present in such a scheme.

$$E(t) + \alpha E(t-\tau) \Leftrightarrow E(\omega) + \alpha E(\omega) e^{i\omega\tau} \tag{13}$$

,

where α is the contrast in peak heights in the double pulse. Therefore, the phase of the double pulse is given by:

$$\varphi(\omega) = \tan^{-1}\left[\frac{\alpha \sin(\omega\tau)}{1 + \alpha\cos(\omega\tau)}\right] \tag{14}$$

.

When $\alpha = 1$, the phase-jump is exactly π. As α decreases, the phase-jumps decrease as well.

3.4 SI to measure weak light pulses

Ultrashort light pulses are very prevalent in nature. Key processes in nature such as photosynthesis, vision, molecular vibrations, liquid-phase collisions all occur on ultrashort time scales. While the pulse-measurement community has mastered the ability to measure ultrashort pulses generated by lasers, we are still learning our way into measuring such vital natural pulses which would increase our knowledge tremendously.

The key to measuring the spectral phase of arbitrary unknown light as generally as one can measure it's spectrum is the use of an extremely broadband reference light wave. And, most importantly, it must have known spectral phase.

The advent of microstructure or photonic crystal fibers about 5 years ago heralded great advances in the field of ultrafast optics. Pulses with bandwidths spanning from 400 nm to 1200 nm could be generated by launching pulses from an 800 nm Ti:Sapphire laser [33]. Unlike the white light continuum generated in bulk media such as a sapphire plate, the white light from a microstructure fiber had a beautiful spatial mode and was spatially coherent. Such stable broadband light sources opened up exciting possibilities as a reference pulse for spectral interferometric experiments in measuring arbitrary ultrashort pulses.

We did some preliminary studies to explore the possibilities of using SI with this broadband reference pulse to measure the weak fluorescence generated in the fluorescent dye

Malachite Green. The dye was found to have a lifetime of about 1.5 picoseconds and a very low quantum yield of $\sim 10^{-4}$. Although the dye has been well-studied there have been no known measurements of its spectral phase, or for that matter, the phase of most fluorescent dyes. However, some ground-breaking experiments in characterizing this broadband "super-continuum" revealed that while the phase of the pulse is extremely stable, the spectrum itself has extremely fine structure on the 1 nm scale, which varies from pulse-to-pulse, making it a difficult choice to use as a reference pulse in interferometric measurements [23, 24, 22].

However, there were other problems in using SI for studying fluorescence which made us abandon this approach to solving the problem of phase measurement of fluorescence. Since fluorescence pulses varied from shot-to-shot, we had to perform spectral interferometry on a single-shot basis. This meant that the sensitivity of the technique was now brought down from the zeptoJoule regime to the attoJoule regime for an oscillator system, with its 100s of MHz repetition rate. Since fluorescence pulses were also spatially incoherent, the number of coherent fluorescence photons collected were severely limited (according to the Van Cittert-Zirneke theorem [4, 42, 46]). These two constraints together put a severe limitation on the number of fluorescence photons that we were able to collect from a low quantum-yielding sample. In conjunction with the fact that our reference pulse appeared to be highly structured, this made Spectral Interferometry an impractical technique to use to measure fluorescence pulses.

Completing a full circle, theoretical simulations [21] and experiments [18] have since then shown that it is possible to generate smoother super-continua using shorter microstructure fibers of ~ 1 cm length, which might be more suitable as reference pulses in SI experiments. Also, the advent of very high resolution *and cheap* fiber spectrometers as well as higher repetition rate amplifiers makes this problem worth revisiting again.

CHAPTER 4

CROSS-CORRELATION FREQUENCY RESOLVED OPTICAL GATING

Sections of this chapter originally appeared as a paper by the author:

J. Y. Zhang, A. P. Shreenath, M. Kimmel, E. Zeek, R. Trebino, and S. Link, "Measurement of the intensity and phase of attojoule femtosecond light pulses using optical-parametric-amplification cross-correlation frequency-resolved optical gating," Optics Express 11(6), 601-609 (2003). [48]

4.1 Introduction

The FROG technique, a self-referencing technique, usually allows us to measure an ultrashort pulse in the absence of a shorter reference pulse. But if a shorter well characterized pulse is already available, it is usually preferable to use this pulse as a reference pulse in order to measure the unknown pulse. In fact, even if the reference pulse is not shorter than the pulse it be measured, it may still be advantageous to use it to measure the reference pulse. For instance, the efficiency of the nonlinear optical process can be increased by using a reference pulse which is highly intense, even if it happens to be longer than the unknown pulse. This increases the sensitivity of the pulse measurement technique and allows pulses that were previously immeasurable - because of how weak they were - to be measured. In addition, XFROG traces generated by gating the unknown pulse with smoother reference pulses are intuitive to interpretation, without having to apply the XFROG retrieval algorithm. This is particularly useful if the unknown pulse happens to be complex.

The process of gating the unknown pulse with a known (different) pulse is known as Cross-Correlation. Spectrally resolving the cross-correlation signal is termed Cross-correlation Frequency Resolved Optical Gating or XFROG [28]. In the past researchers have performed spectrally resolved cross-correlation in order to study unknown pulses. They

have been able to measure the pulse color as a function of time using this technique. The resulting spectrogram, made using a shorter reference pulse, is very intuitive in understanding the nature of the unknown pulse. However, no one attempted to extract quantitative information about the unknown pulse. Then, in the mid-90's, the FROG-like algorithm was applied to an XFROG spectrogram. It was a big advancement in the field, allowing the intensity and phase of the unknown pulse to be measured - and that is what makes XFROG a powerful tool to investigate unknown weak pulses.

XFROG experiments are easy to set-up and perform. There is no special requirement for the reference pulse, such as in Spectral Interferometry(SI). For instance, the spectrum of the reference pulse does not need to overlap with that of the unknown pulse. Moreover, the absolute phase (the zeroth order phase term) of the pulse need not be the same from pulse to pulse in a pulse train, i.e., the pulses do not need to be temporally coherent. This is because XFROG - like other multishot FROG techniques does not measure absolute phase. This quantity is of little consequence for most experiments. Again unlike SI, XFROG does not have stringent mode-matching requirements. This allows pulses that are not spatially coherent to be measured.

XFROG is also more versatile than other pulse measurement techniques. Depending on the relative frequencies between the reference pulse and the unknown pulse, XFROG geometries can be adapted to different nonlinearities, such as the sum frequency generation (SFG), difference frequency generation (DFG), optical parametric amplification (OPA) or even third order processes such as self diffraction (SD) and polarization gating (PG) XFROG.

XFROG has several "trivial" ambiguities. As previously mentioned, the usual absolute phase ambiguity that is common to all FROG techniques. This is trivial however since the absolute phase term is not a very important physical quantity in most experiments. However, unlike FROG measurements, where there is a translation ambiguity present that makes the origin of the time axis somewhat arbitrary XFROG measurements display a fixed time axis with respect to the gate pulse.

Finally, the XFROG trace that is generated is not usually symmetric and hence offers an

intuitive understanding of the unknown pulse as a function of time. This helps rule out the direction-of-time ambiguity - to some degree. It must be kept in mind that if the reference pulse had been characterized using SHG FROG or GRENOUILLE, then there is a possible time ambiguity present in the characterization of the reference pulse itself. However, it is very easy to eliminate such time ambiguities in a SHG FROG measurement as discussed previously in chapter 2. Of course, the direction of time ambiguity in the gate pulse is pretty obvious during an XFROG trace retrieval, since the retrieved XFROG trace differs appreciably from the measured XFROG trace and the XFROG error is large.

4.2 Theoretical background

4.2.1 XFROG

The general expression for such an XFROG trace is:

$$I_{XFROG}(\omega,\tau) = \left| \int_{-\infty}^{\infty} E(t) E_{gate}(t-\tau) \exp(-i\omega t)\, dt \right|^2 \tag{15}$$

where the gate function, $E_{gate(t)}$, can be any function (i.e., pulse) that happens to be available and which has temporal structure on the order of that of the pulse to be measured, E(t). If $E_{gate(t)}$ is a function of E(t) itself, the method is FROG; if not, it is XFROG. All that is required is a signal field that is a function of time and delay, an example of which is a product of the form, $E(t)E_{gate(t-\tau)}$, which can then be spectrally resolved.

SFG XFROG is the most obvious of the XFROG geometries to be used in experiments. Frequency Upconversion, a widely used technique to study fluorescence, is in fact the process of sum frequency generation. The sum frequency signal can readily be generated by gating the unknown pulse with the pulse from the Ti:Sapphire laser which acts as the reference pulse. The gate function in the XFROG signal then takes the form:

$$E_{gate} = E_{ref} \tag{16}$$

The carrier frequency corresponding to the sum frequency signal is $\omega_{SFG} = \omega_{unk} + \omega_{ref}$. If it were inconvenient to measure the sum frequency signal, say because it was too far in the UV, for instance, then it would be more practical to use difference frequency generation

to measure the signal. In this case, the carrier frequency would correspondingly be $\omega_{DFG} = \omega_{unk} - \omega_{ref}$. DFG XFROG will be discussed in greater detail in the following section.

It can be seen from the above equations that the XFROG signal is proportional to the squared magnitude of the reference pulse. This is responsible for the heterodyne property of the XFROG technique, which allows weaker pulses to be measured as compared to the FROG technique.

4.2.2 DFG-XFROG and OPA-XFROG

While the idea of DFG XFROG has been around for at least the last five years, no previous attempt had been made to exploit the one obvious difference between the process of DFG and other second order nonlinear processes during XFROG measurements - that of exponential gain in signal and idler intensity that occurs during the DFG interaction [29]. The theory behind difference frequency generation is well understood [6, 3, 35]. This section will discuss the simple theory behind DFG and OPA. Here we make a series of simple assumptions to derive our theory. We start off by assuming that the bandwidths in the pulses are narrow enough compared to the carrier frequencies that we can approximate the pulses by optical fields of infinite uniform plane waves at the carrier frequencies, propagating along the z-axis. These are given by

$$\mathbf{E}_j(\omega_j) = \frac{1}{2} E_j(z) e^{i(k_j z - \omega_j t)} + c.c. \tag{17}$$

where j=s,i,p and $E_j(z)$ represents the complex field amplitude. Substituting for $\mathbf{P}^{(2)}$ and $\mathbf{E}$ in Maxwell's wave equation, we can separate the result into the three components at ω_s, ω_i and ω_p, which will each separately satisfy the wave equation. We also make the assumption that the field amplitudes or "envelopes" vary slowly over distance compared to wavelengths, i.e., apply the so-called "Slowly Varying Envelope Approximation **(SVEA)**" to our equations.

The coupled-wave equations for the generation of the signal and idler (which we will refer to here as the OPA and DFG pulses, respectively, because the term "signal" is already used in FROG and has a different meaning) and the pump are then given by:

$$\frac{\partial E_{OPA}}{\partial z} = i\kappa E_{ref} E^*_{DFG} e^{i\Delta k z} \tag{18}$$

$$\frac{\partial E_{DFG}}{\partial z} = i\kappa' E_{ref} E^*_{OPA} e^{i\Delta k z} \tag{19}$$

and

$$\frac{\partial E_p}{\partial z} = i\kappa_p E_{OPA} E_{DFG} e^{-i\Delta k z} \tag{20}$$

where $\kappa = \frac{4\pi d_{eff}}{n_{OPA}\lambda_{OPA}}$, $\kappa' = \frac{4\pi d_{eff}}{n_{DFG}\lambda_{DFG}}$ and $\kappa_p = \frac{4\pi d_{eff}}{n_p \lambda_p}$ and $\Delta k = k_p - k_{OPA} - k_{DFG}$. Here we also assume that the process is completely phase-matched, so that we can set $\Delta k = 0$. Finally we follow the convention that the d-coefficient is related to the susceptibility tensor as:

$$d_{ijk} = (\frac{1}{2})\chi^{(2)}{}_{ijk} \tag{21}$$

The general solutions to these equations are difficult, but assuming that the pump depletion is negligible, eqn. (20) yields $E_p = constant$. The electric field of the signal pulse emerging from the crystal in an OPA XFROG apparatus then has the form:

$$E^{OPA}_{sig}(t,\tau) = E(t)\, E^{OPA}_{gate}(t-\tau), \tag{22}$$

with $E(t)$ as the unknown input pulse. The second factor is the gate pulse, which we solve using equation (18). It is given by

$$E^{OPA}_{gate}(t) = \cosh(g\,|E_{ref}(t)|\,z) \tag{23}$$

Here, the gain parameter, g, is given by:

$$g^2 = \frac{16\pi^2 d^2_{eff}}{n_{OPA} n_{DFG} \lambda_{OPA} \lambda_{DFG}} \tag{24}$$

Thus, from equation(23), it can be seen that the pulse to be measured undergoes exponential gain during OPA and retains its phase during the process of OPA.

Note that in the experiments, when we refer to gain, we will actually be referring to the net gain that a seed pulse sees as a result of the gain parameter acting along the length of the crystal L. Since the process is phase-matched, the net gain is given by:

$$G \simeq (gL)^2 \tag{25}$$

The setup for DFG XFROG is similar to that of the OPA XFROG, except that now the idler is imaged onto the slit of the spectrometer to yield a DFG XFROG trace. Although it is known that DFG XFROG is a sensitive technique for measuring fairly weak pulses [29], the method has never been demonstrated with gain. Here we consider the effect of possible gain so that the electric field is given by:

$$E_{sig}^{DFG}(t,\tau) = E(t)\, E_{gate}^{DFG^*}(t-\tau) \tag{26}$$

This has the same unknown input pulse and a gate function of the form:

$$E_{gate}^{DFG}(t) = \exp[i\phi_{ref}(t)] \sinh(g\,|E_{ref}(t)|\,z) \tag{27}$$

where $\phi_{ref}(t)$ is the phase of the reference pulse. In the limit that the reference pulse is weak, the net gain is small, and the above expression reduces to $E_{gate}^{DFG}(t) = E_{ref}(t)$. This then brings the expression for the signal pulse to the more familiar form

$$E_{sig}^{DFG}(t,\tau) = E(t)\, E_{ref}^{*}(t-\tau) \tag{28}$$

The measured XFROG trace is the magnitude-squared Fourier transform of the various signal fields. In both OPA and DFG XFROG, the unknown pulse can be easily retrieved from the measured trace using the iterative XFROG algorithm, modified for the above expressions for the gate pulse.

4.3 Experiment

4.3.1 Apparatus

Our experimental setup for OPA/DFG XFROG is shown in figure (23). In our experiments, the output from a femtosecond KM Labs Ti:Sapphire oscillator is amplified using a kilohertz

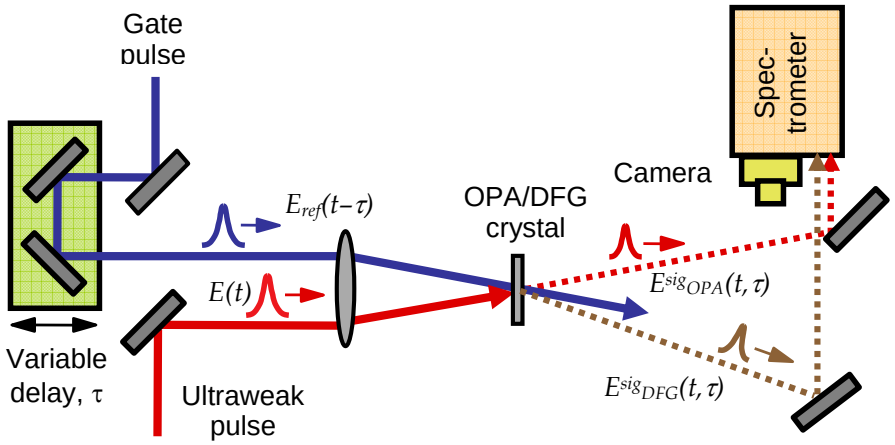

Figure 23: Schematic of the experimental apparatus for OPA/DFG XFROG. The gate pulse is characterized using a GRENOUILLE (not shown) before it enters the XFROG setup.

repetition rate Quantronix regenerative amplifier. The amplified 800 nm pulse is then characterized using a Swamp Optics GRENOUILLE. The pulse is then split into two.

One pulse is used to generate a white-light continuum (with poor spatial coherence) in a 2-mm thick sapphire plate. This is then spectrally filtered to yield a narrow slice of the spectrum about 3 nm wide around 600 nm. The pulse is measured to have $\sim$ 80 picojoules(pJ) of energy. The pulse is then attenuated using a 3.0 OD neutral density filter by a factor of 1000, so that it has an energy of about 80 femtojoules(fJ). It is the "unknown" pulse in our experiments.

The other pulse from the beam-splitter is frequency-doubled in a 1-mm thick BBO crystal using Type I phase matching and passed through a variable time delay to act as a gate (pump) pulse (with 5.8 μ J) for the OPA/gating process.

The two pulses are focused by a single 75-mm spherical mirror at a small angle (3°) in a 1-mm thick BBO crystal, again using Type I phase matching conditions. It must be pointed out that the interaction here is considered Type I although the two input beams are of different polarizations. Here the unknown pulse has 'o' polarization, while the bluer pump pulse has 'e' polarization. The idler pulse which is generated as a result of this process exits with 'o' polarization.

The thickness of the crystal is chosen so that the equations from the previous section are still applicable. This crystal thickness is also sufficient to accommodate the phase-matching bandwidth of the weak pulse. The thickness also ensures that the group velocity mismatch (GVM) between the various pulses is minimized during the interaction. This will be discussed in greater detail in the following chapter.

The signal at the CCD array is integrated over a few seconds. The OPA signal emerging from the BBO crystal sees an average gain (G) of about $\cosh(5.75) \simeq 150$, which, in view of the weak pulses involved, easily satisfies the condition of negligible pump depletion. This value of the gain is, however, more than sufficient to record the spectrally dispersed signal at the camera, i.e., the OPA spectrum vs. relative delay, which is the OPA XFROG trace.

4.3.2 Results

Using OPA XFROG, we first measured the above-described 80 fJ pulse. The calculated second harmonic of the pulse from the amplifier, which had been characterized using the Swamp Optics GRENOUILLE was used as the reference pulse. Figure (24) shows the measured and retrieved OPA XFROG trace for this pulse, along with the retrieved intensity and phase vs. time and the spectrum and spectral phase vs. wavelength. The FROG error was 0.01 for this 128 x 128 pixel trace. The retrieved pulse had a temporal intensity Full Width Half Maximum (FWHM) of 266.5 fs. The spectral FWHM was 2.428 nm, so that the FWHM time-bandwidth product (TBP) was 0.4976.

To verify the results of the above newly introduced OPA XFROG measurement, we measured the same continuum pulse using a well established, but less sensitive, method: SFG XFROG (see figure (24)). The experimental setup was similar to that of OPA XFROG, with a few minor variations. The 800 nm fundamental pulse from the amplifier acted as the reference pulse for the SFG process. It was attenuated to 400 nJ. Also, since SFG XFROG is a less sensitive technique than OPA XFROG, the continuum was now un-attenuated and so the unknown pulse had a pulse energy of 80 pJ. Also a 100 micron thick Type I BBO crystal was used to phase-match the sum frequency signal. The resulting sum-frequency signal was imaged onto an Oriel spectrometer.

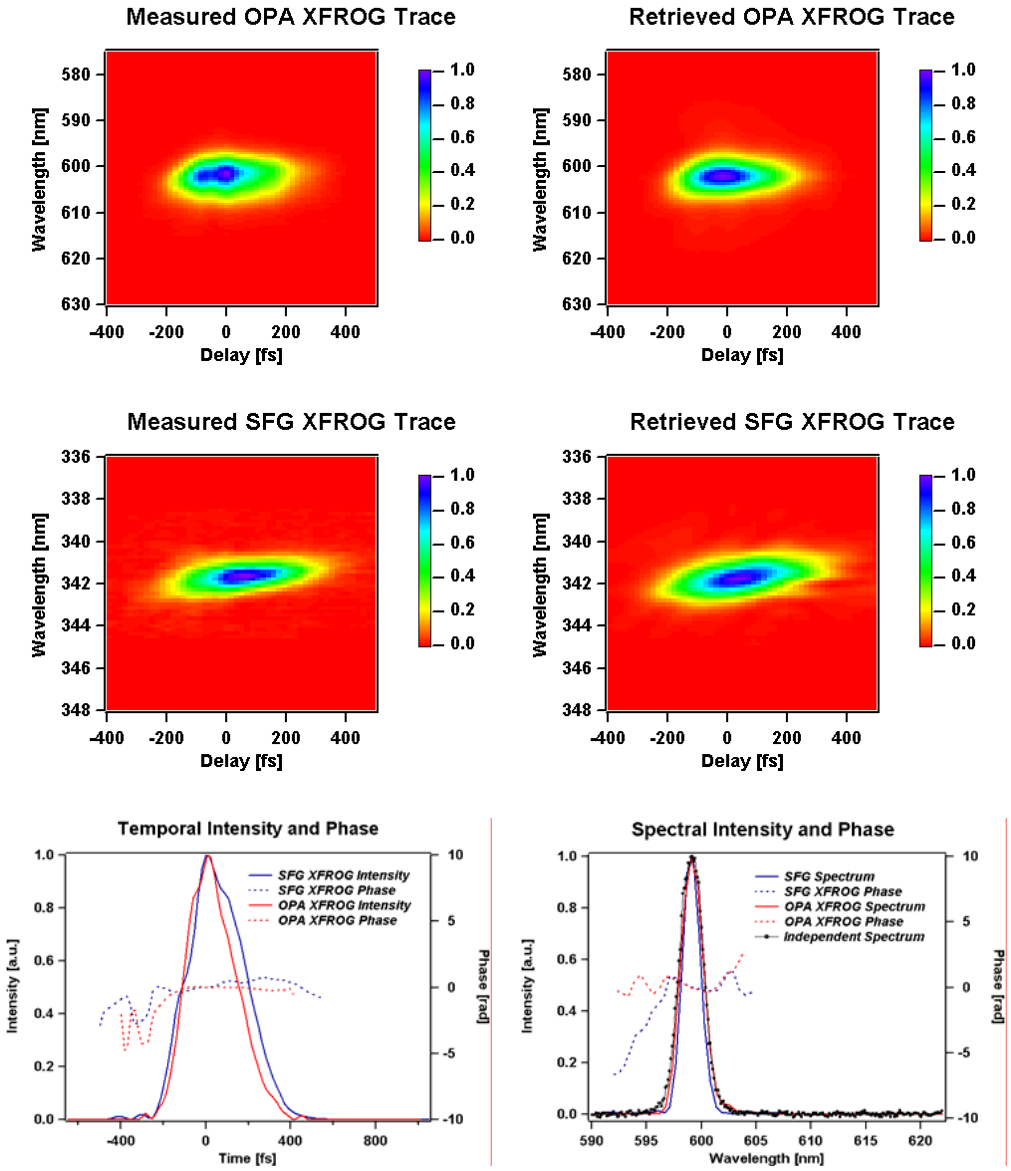

Figure 24: The measured and retrieved traces and retrieved intensity and phase vs. time and the spectrum and spectral phase vs. wavelength of a spectrally filtered continuum from a sapphire plate. The retrieved intensity and phase from the OPA XFROG measurement of 80fJ pulses agrees well with the retrieved intensity and phase of unattenuated continuum of 80pJ using the established technique, SFG XFROG as well as the independently measured spectrum.

For the SFG measurement, the retrieval on a 128 x 128 trace had a FROG error of 0.014. The temporal intensity FWHM was 284.4 fs and the spectral FWHM was 2.056 nm, so that the FWHM TBP was 0.4498. The two measurements of the same pulse agreed reasonably well.

In addition, the spectrum of the "unknown" pulse was measured independently using the spectrometer. This spectrum also matched the retrieved spectrum from the XFROG measurements. The results from this experiment established OPA XFROG as a reliable ultrafast pulse measurement technique. Also this experiment showed that OPA XFROG could reliably measure pulses at least three orders of magnitude weaker than those measured using SFG XFROG.

The temporal resolution of any XFROG trace is not restricted by the pulse width of the reference pulse. This is because information from both the temporal and spectral domains of the reference pulse *and* the unknown pulse are simultaneously contained in the XFROG trace. A short reference pulse would yield good temporal resolution of the unknown pulse but wash out spectral features as a result of the broad bandwidths contained in the reference pulse. Of course, a reference pulse with a narrow spectrum would mask temporal features while providing good spectral resolution. While each such measurement would in and of itself be adequate, it is better to find a happy medium and distribute the information more evenly in both the temporal and spectral domains. This is where OPA XFROG shows another distinct advantage over other XFROG techniques.

Since the reference pulse appears in the exponent of the gate function, the net effect is that of a narrower gate pulse than the reference pulse providing us with a finer temporal resolution. This is a desirable effect, although the spectral resolution is slightly compromised.

4.4 Optical Parametric Generation

Optical Parametric Generation(OPG) is a spontaneous process that is often referred to as Super-fluorescence. When an intense photon of frequency ω_p is incident on a nonlinear medium, it sometimes splits into two lower-frequency (and hence weaker) photons, satisfying

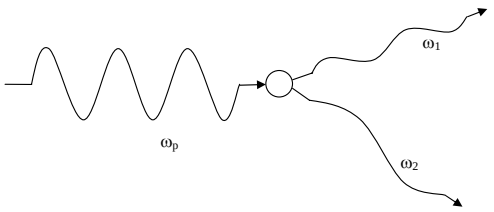

Figure 25: Spontaneous parametric fluorescence where the pump of energy $\hbar\omega_p$ breaks up into two photons of energy $\hbar\omega_1$ and $\hbar\omega_2$

the conservation of energy equation $\omega_p = \omega_1 + \omega_2$, as shown in figure (25). OPG is a completely quantum mechanical effect first predicted and studied by Louisell et al [30]. Its theory can however be treated semiclassically, since the intense pump photon can be approximated to a constant classical field. Perturbation theory can be applied to calculate the expectation values of the emerging lower frequency fields. A detailed discussion of such a calculation is beyond the realm of this thesis. However, the result of such calculations, i.e., the expectation values for the emerging frequencies quoted in the equations below.

$$\langle n_i(t)\rangle = \langle n_p(0)\rangle \cosh^2\left(\tfrac{1}{2}G_0 t\right) + (1 + \langle n_q(0)\rangle)\sinh^2\left(\tfrac{1}{2}G_0 t\right) \tag{29}$$

where $p, q = 1, 2$ and $p \neq q$. Here the Gain coefficient G is given by:

$$G_0 = 8\pi d_{eff}\sqrt{\frac{cI_p(0)}{2\varepsilon_0 n_p n_1^2 n_2^2 \lambda_1 \lambda_2}}\frac{\sin\left(\Delta k L/2\right)}{\left(\Delta k L/2\right)} \tag{30}$$

Note that from the equation for the expectation values, even when there are no input photons other than the pump itself, (i.e., $\langle n_p(0)\rangle = 0$), OPG photons are still generated. This can be seen from the unity factor in eqn. 29. Thus, this is the spontaneous emission term.

Although conservation of energy permits the lower frequency photons to have any value from 0 to ω_p radiated in any direction, in reality, phase-matching conditions decide the frequency and direction of emergence of the lower frequency photons. In other words, phase-matching conditions decide at what frequencies the gain occurs, as can be seen from eqn. 30. And *this* plays an important role in the OPA XFROG experiments. A small

amount of phase mismatch is tolerated by the process. OPG frequencies satisfying these conditions emerge from the nonlinear crystal as a cone subtending an angle 2θ around the pump beam. As the crystal angle is changed, the cone expands to redder colors or shrinks to bluer colors, spanning the entire visible spectrum from near ω_p up to the degeneracy wavelength $\omega_{degen} = \omega_p/2$.

4.4.1 Impact of OPG on OPA XFROG measurement

OPA can be thought of as a special case of the process of OPG, where one of the lower frequency photons, the "seed" photon has been supplied as input along with pump pulse. Therefore the phase matching conditions in the experiment is optimized for maximum gain at that particular input frequency ω_s. Obviously, these same conditions will also cause OPG to be generated and optimized at this identical frequency. This OPG now acts as a noise background in the OPA XFROG experiment. This sets a limit on the gain available in OPA XFROG. If the gating pump pulse is too intense, it results in a strong OPG in the nonlinear crystal, which is generated from noise photons and is an unwanted background for the OPA signal. Since, for very high gain, OPG can rival OPA in intensities, this could result in distortion in the XFROG retrieved pulse. Thus, in our experiments, we have to keep the pump power low enough to avoid distortions due to potential OPG background. OPG also places a limit (a few photons per pulse) on how weak the unknown signal can be and still be measured accurately.

4.5 Measuring ultrashort pulses trains of about 150 photons per pulse using OPA-XFROG

In order to test the limits of the OPA XFROG technique, we measured a train of attojoule pulses (only a few hundred photons per pulse). The set-up for the experiment was similar to the one described in the previous chapter. The white light continuum generated in a 2-mm thick sapphire plate was filtered and then attenuated with the help of neutral density filters. Assuming that the ND filters were linear, the pulse train had pulses of energy of 50 attojoules (aJ) per pulse, at a kilo-hertz repetition rate. That corresponds to a pulse train with about 150 photons per pulse at about 575 nm. The OPA process was induced in a

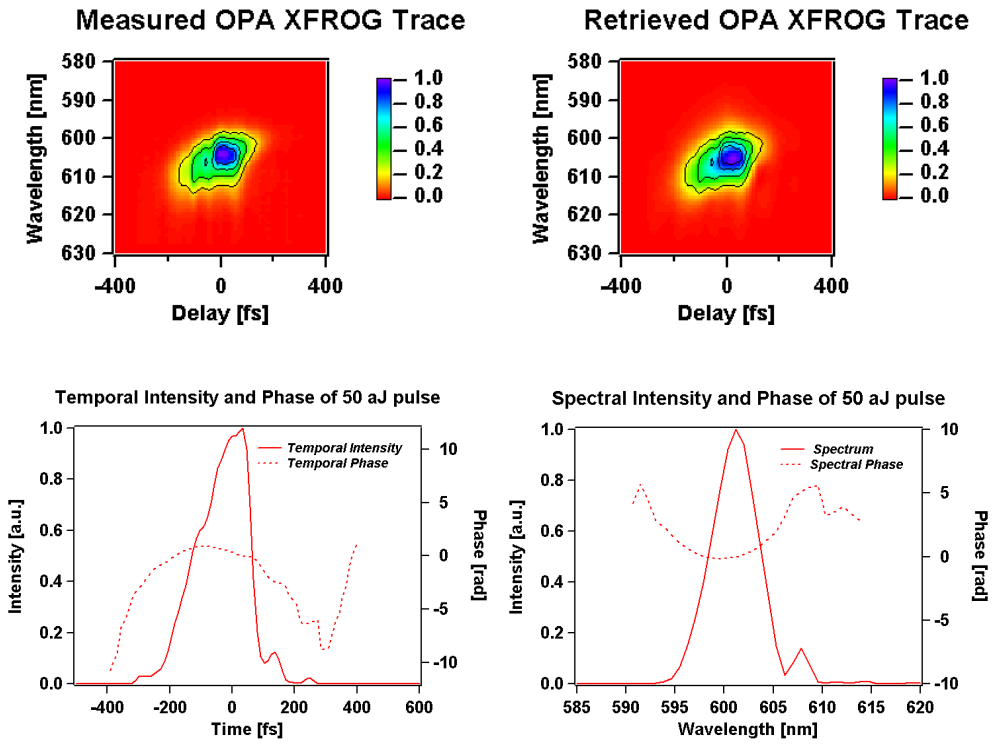

Figure 26: OPA XFROG measurement of a 50 aJ attenuated and filtered continuum generated using a sapphire plate.

2-mm thick BBO crystal.

Our OPA XFROG measurement of the 50 aJ pulse is shown in figure (26). The gain here was about $\cosh(9) \simeq 4000$. The OPA signal intensity in this trace was only ~ 5 times stronger than the OPG background measured on the CCD camera.

In this measurement, for an integration time of one second per delay step, the OPA gain was high enough to saturate the CCD array and so the signal had to be attenuated before entering the spectrometer. In practice, however, the gain should not be so high that such attenuation is required, but allowing it to occur here provided an additional test of the method.

As a result of the very high gain, the OPA XFROG trace showed large fluctuations in

signal strength from one step to the next. This was due in part to variations in the gate-pulse energy (generated in a χ_2 process from the somewhat unstable output from a regenerative amplifier) and from the inherent instability of a single pass OPA process with high gain. Fortunately, the OPA XFROG retrieval algorithm sees through this artifact (which cannot correspond to any real trace structure) and smoothes it out during the retrieval. The retrieved pulse had a temporal intensity FWHM of 170 fs and a spectral FWHM of 5.165 nm, with a FROG error of 0.0146 on a 128 x 128 grid. The corresponding TBP was 0.731.

As can be seen from a comparison of the measured and retrieved XFROG traces, the FROG error is very low considering how weak the signal pulse is. The OPA XFROG technique is very robust as it can faithfully measure pulses which have an intensity signal to noise ratio of only about five. It can also measure extremely weak pulses. In fact, OPA XFROG is currently the most sensitive ultrafast pulse measurement technique. This demonstration does better than the Spectral Interferometry measurements mentioned in Chapter 3, since those zeptoJoule(zJ) pulse measurements were performed with a Ti:Sapphire oscillator, whose repetition rate was about 5 orders of magnitude higher than that of the regenerative amplifier used in our aJ OPA XFROG measurement, so that the input power of our signal photons were a factor of 10 less than that of the Spectral Interferometry measurement.

CHAPTER 5

NON-COLLINEAR OPTICAL PARAMETRIC AMPLIFICATION

Sections of this chapter originally appeared as a paper by the author:

X. Gu, S. Akturk, A. Shreenath, Q. Cao, and R. Trebino, "The measurement of ultrashort light pulses - Simple devices, complex pulses," Optical Review 11(3), 141-152 (2004). [22]

5.1 Introduction: Phase Matching and Group Velocity Mismatch

Optical parametric processes are second-order nonlinear processes involving the interaction between three optical fields, the pump, signal and idler, with frequencies satisfying equation $\omega_{signal} = \omega_{pump} - \omega_{idler}$, in a $\chi^{(2)}$ nonlinear medium. Under suitable phase-matching conditions, the generated signal and idler undergo huge amplification by draining the pump field of its power as they propagate through the nonlinear crystal.

It can be seen from equation (24,25) that the magnitude of nonlinear gain depends on several material parameters such as refractive index, nonlinear coefficient, crystal length, signal and idler wavelengths as well as pump intensity at the input of the nonlinear crystal. However, in deriving these equations, we made the assumption that the process was phase-matched, so that we could set $\Delta k = 0$ giving us conditions for maximum gain. It is now time to examine this issue in detail and deal with its implications to the OPA XFROG measurements.

The general functional dependence of gain on Δk can be found in a number of reference texts [6, 35]. In most practical situations, when pump depletion is negligible, the conversion efficiency is low and the pump is constant. The conversion efficiency is found to depend on the phase-matching bandwidth as

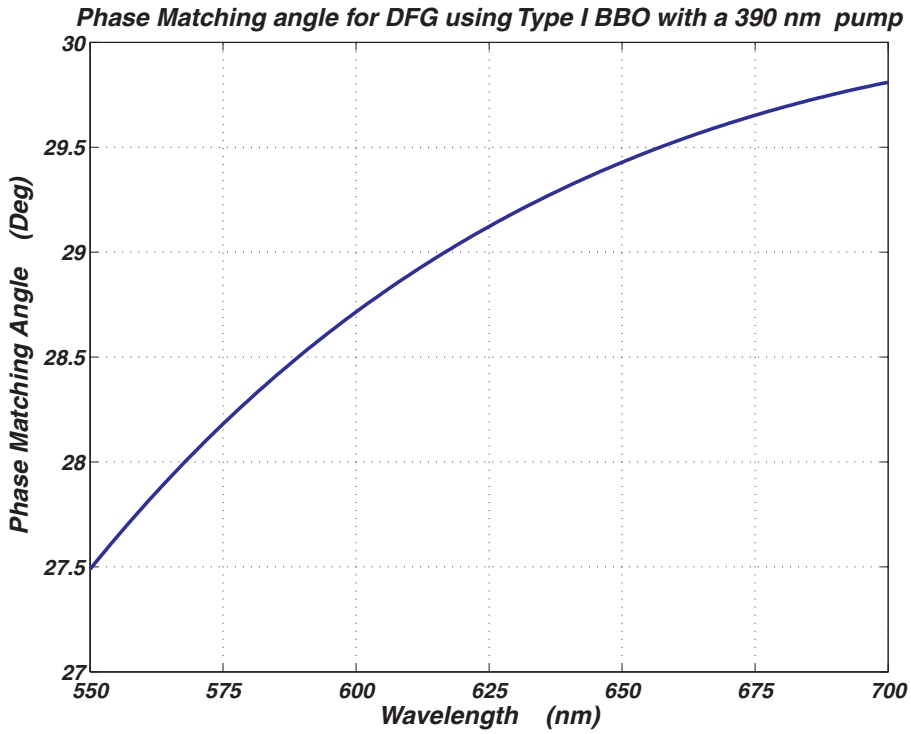

Figure 27: Phase Matching Angles are calculated for the nonlinearity of DFG with the pump pulse at 390 nm. BBO is used in type I configuration for this calculation. The phase matching angles span over 2.25° for a wavelength range of about 150nm.

$$\frac{\mathcal{P}_{out}}{\mathcal{P}_{in}} \propto \frac{sin^2(\Delta kL/2)}{(\Delta kL/2)^2} \tag{31}$$

.

The $sinc^2(\Delta kL/2)$ dependence in this formula describes the effects of unequal phase velocities of the interacting waves. Of course this dependence of efficiency on $sinc^2(x)$ is not restricted to DFG alone. If $\Delta kL/2$ is not close to zero, the efficiency of the process drops significantly. A plot of the relevant phase-matching angles and the resulting phase-matching efficiency for OPA XFROG using a 390nm pump is given in figures (27) and (28) respectively. It can be seen from figure (27), that a signal centered at about 615nm phase-matches close to 29°. At this angle, we can phase-match 5.7 nm of bandwidth at most, if we use the 2mm BBO, in a Type I configuration, when the pump and seed are collinear. However, if we change the phase-matching angle to 29.5°, we now can phase-match almost 9nm around 660 nm. Similarly, if we change the phase-matching to 28.5° we phase-match

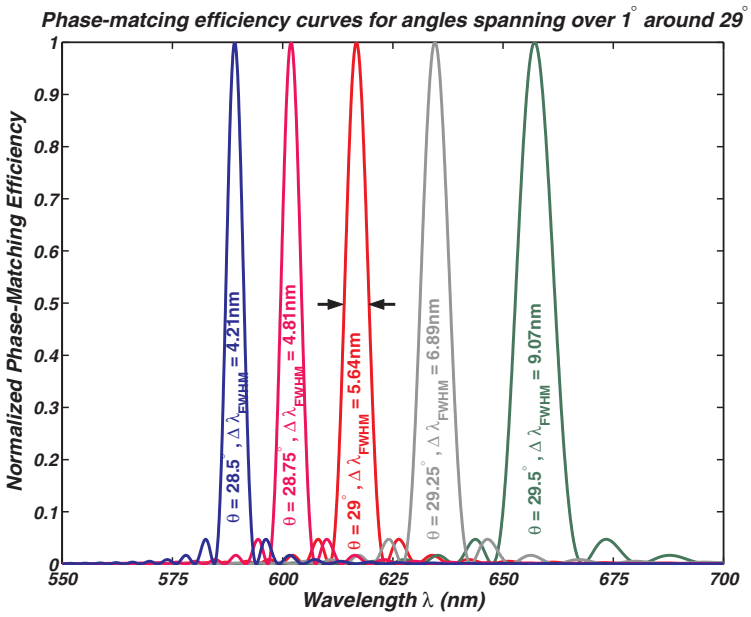

Figure 28: Phase Matching Efficiency is calculated for a range of phase matching angles ranging from 28.5° to 29.5°, for the OPA XFROG process with the pump pulse at 390 nm.

a 4.2nm bandwidth about 583nm.

In our experiment, when we focus into the crystal to increase intensity, we in fact improve the phase-matching bandwidth at each of the phase-matching angles. There are several studies that indicate that focusing beams into nonlinear crystals show an almost 10-fold increase in phase-matching bandwidth [5, 2]. This allows us to consider using OPA in a regime involving broad bandwidth femtosecond pulses.

In practice, we do not see such large bandwidth increases when we focus tightly into a crystal because the coherence length, given by

$$\mathbf{L}_c = \frac{2\pi}{|\Delta k|}, \tag{32}$$

is very small for such a large bandwidth. Also, in addition to phase-velocity matching, it now becomes necessary to consider the effect of group-velocities during the propagation of these pulses.

The larger the bandwidth of the pulse to be measured, the larger will be the group-velocity mismatch (GVM) and the shorter the actual interaction length is between the

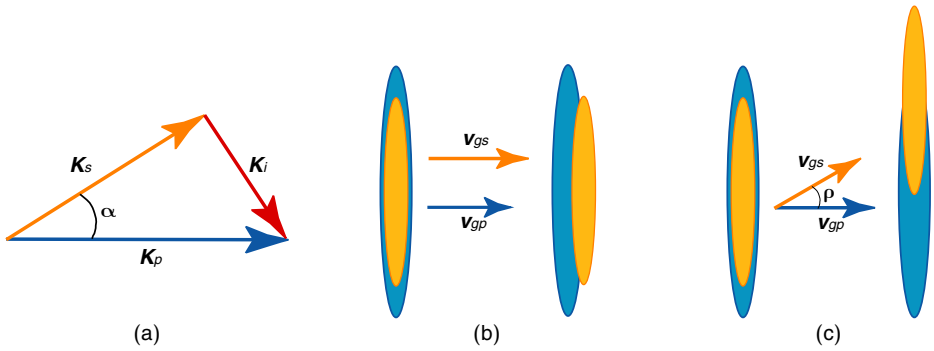

Figure 29: (a) Schematic for a non-collinear geometry in OPA XROG; (b) Representation of signal and pump pulses in case of a collinear set-up; (c) The same case as (b) in a non-collinear set-up.

pulses. Defining the pulse-splitting length l_{sp} [7] as the propagating distance after which the pump and the seed pulses separate from each other by a pulse length,

$$l_{sp} = \frac{\tau_p}{GVM_{sp}} \tag{33}$$

,

where τ_p is the length of the longer of the seed or the pump. GVM effects can be neglected to a first approximation when the crystal lengths are shorter than l_{sp}.

However, alternately, in such a situation, we see that an additional degree of freedom can be introduced by switching from a collinear geometry in the set-up to a non-collinear geometry [8, 37, 34, 26, 13, 11, 12, 10, **?**]. This is shown in figure (29). Independent of wavelength, the pump and seed pulses are made to cross at an angle α. If the resulting angle between the pump and idler is referred to as β, then, the phase-matching condition is now a vector equation, which can be decomposed into:

$$\begin{aligned} \Delta k_{\parallel} &= k_p - k_s \cos\alpha - k_i \cos\beta = 0 \\ \Delta k_{\perp} &= k_s \sin\alpha - k_i \sin\beta = 0 \end{aligned} \tag{34}$$

.

The angle β is not fixed but depends on the seed wavelength. If the seed frequency increases by $\Delta\omega$, the idler frequency correspondingly decreases by $\Delta\omega$. The wave vector mismatch along the two direction can be approximated, to the first order, as

$$\begin{aligned}\Delta k_{\parallel} &\cong -\frac{\partial k_s}{\partial \omega_s}\cos\alpha\ \Delta\omega - \frac{\partial k_i}{\partial \omega_i}\cos\beta\ \Delta\omega + k_i \sin\beta \frac{\partial \beta}{\partial \omega_i}\ \Delta\omega \\ \Delta k_{\perp} &\cong \frac{\partial k_s}{\partial \omega_s}\sin\alpha\ \Delta\omega - \frac{\partial k_i}{\partial \omega_i}\sin\beta\ \Delta\omega - k_i \cos\beta \frac{\partial \beta}{\partial \omega_i}\ \Delta\omega\end{aligned} \tag{35}$$

.

Since to achieve broadband phase-matching, both $\Delta k_{\parallel}$ and $\Delta k_{\perp}$ must vanish individually, we get the following condition:

$$v_{gi} = -v_{gs}\cos(\alpha + \beta) \tag{36}$$

.

Thus, broadband phase-matching and group-velocity matching can be simultaneously achieved if the projection of the idler group velocity on to the seed direction equals the group velocity of the seed. This effect is shown schematically in figure (29(b)) for the pump and seed travelling collinearly at different group velocities which cause them to separate quickly, resulting in pulse lengthening and bandwidth reduction. For the non-collinear case in figure(29(c)), the two pulses stay overlapped effectively, although there is a (spatial) walk-off of the seed with respect to the pump direction. Figure(30) shows the broadband amplification achieved in a NOPA geometry as opposed to a collinear OPA set-up.

SNLO, a freeware available on the internet, by A. V. Smith allows for the calculations of suitable crossing angles and phase-matching angles to minimize GVM, for wavelengths of interest [36].

The conversion efficiency of the OPA XFROG process is affected by this beam "walk off". In birefringent media, the direction of propagation for an extraordinary wave is different in general from that of the ordinary wave (i.e., energy propagation). Thus, the ordinary and extraordinary beams of finite spot size do not overlap completely through the entire length of the crystal. The extraordinary beam is said to "walk off" from the ordinary axis at an angle ρ called the walk-off angle. In a uniaxial crystal such as BBO, this walk-off angle depends on the refractive index of the crystal as

$$tan\rho = \frac{[n^e(\theta)]^2}{2}[\frac{1}{(n^e)^2} - \frac{1}{(n^o)^2}]sin2\theta \tag{37}$$

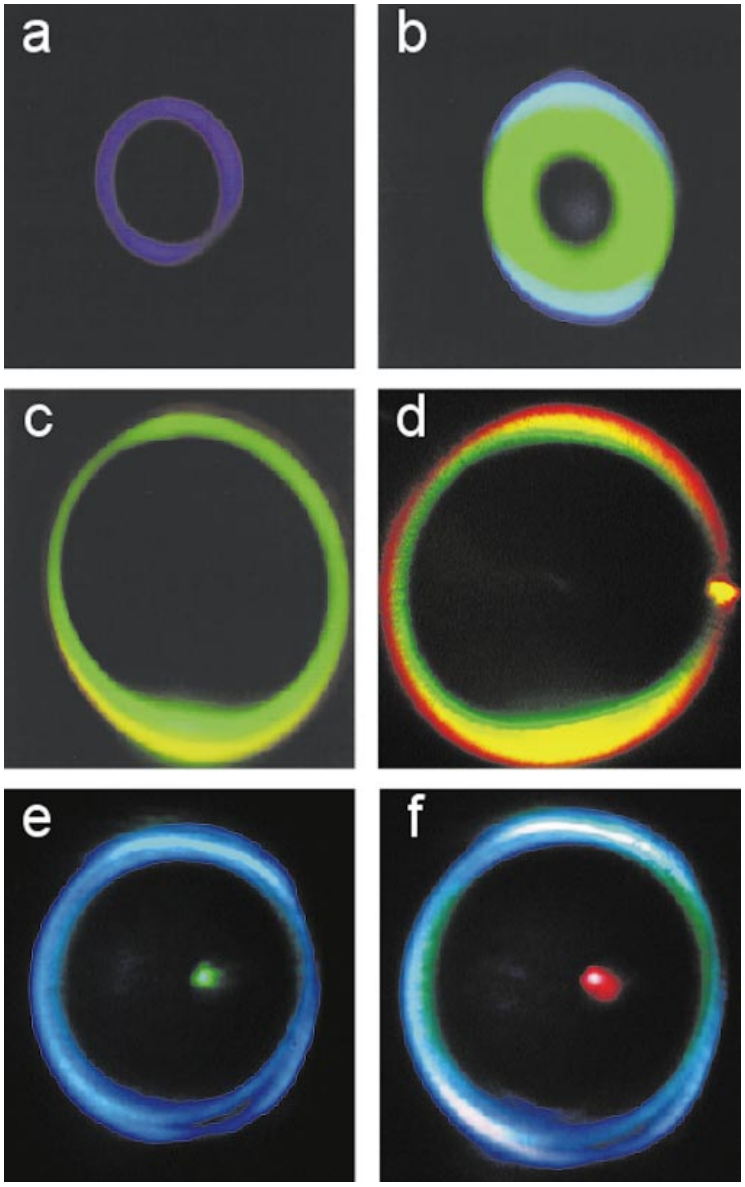

Figure 30: Photographed images of parametric signal wave at the output of a BBO crystal [26]. (a-c) Non-collinear OPG at phase-matching angles of $\theta = 25°, 29°$ and $31.7°$ respectively. (d) NOPA with continuum seed crossing at $\alpha \approx 3.1°$ for $\theta = 29°$. (e,f) Collinear OPA at $\theta = 25.5°$ and $27.7°$ respectively.

.

Even for small walk-off angles, the loss in conversion efficiency can be significant. This is because beams that do not spatially overlap cannot participate in the nonlinear process. Since focused beams have decreased dimensions, they can become displaced from each other over very short distances with the nonlinear crystal. So the crystal thickness and focusing parameters are chosen to keep the walk-off to a minimum during the interaction. This may limit the resulting gain as well as effective bandwidth that is phase-matched during OPA.

Thus, we see that if a suitable crossing angle α is chosen between the pump and seed, it is possible to still match the group velocities of the various pulses in order to achieve broadband phase-matching. This effect has been used to advantage by the OPA community and commercially built NOPAs are now available.

5.2 NOPA XFROG: Experimental Results

The schematic for our NOPA XFROG experiment is as show in figure (23). In this experiment, we chose to cross our pump and seed pulse from the white light continuum at an angle of $\sim 6.5^\circ$ (internal in the crystal), chosen in order to minimize GVM.

The pump pulse was generated as before by doubling the output from the regenerative amplifier using a 1-mm thick Type I BBO crystal. The amplifier pulse was characterized using a Swamp Optics GRENOUILLE and its E-field doubled to yield the pump "reference" pulse. The conversion efficiency was deliberately kept low at 15%, in order to minimize OPG effects. A harmonic separator was then used to separate out the fundamental pulse from the second harmonic pulse.

The broadband white light continuum, our seed "unknown" pulse, was once again generated by a 2-mm thick sapphire plate, by focusing the harmonically separated 800 nm fundamental beam tightly into the sapphire plate. The resulting white light was then spectrally filtered using a combination of BG40 and OG515 colored glass filters to yield a broadband spectrum about 60 nm centered around 575 nm. These pulses were generated from multiple filament sources in the sapphire plate and hence had relatively poor spatial coherence mimicking the behavior of the spatially incoherent fluorescence sources.

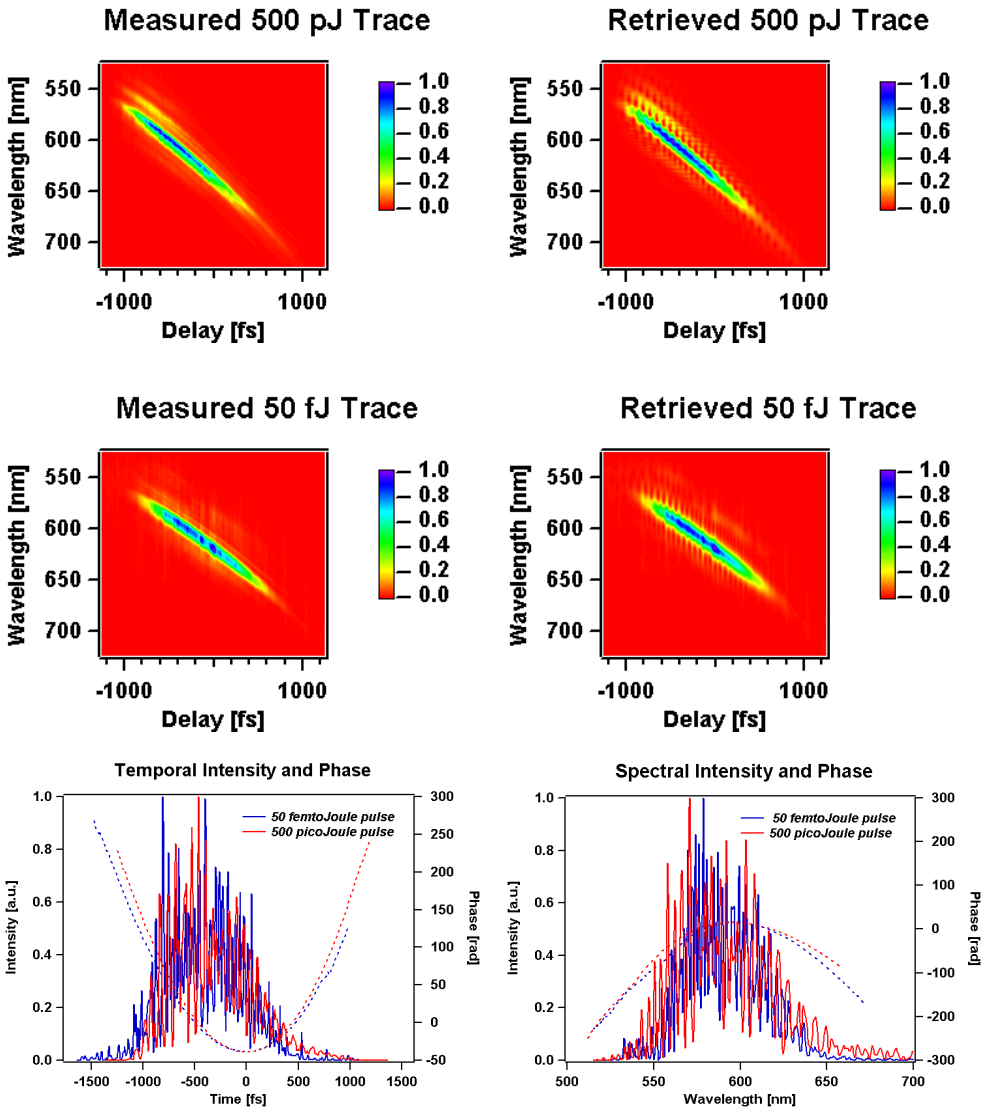

Figure 31: Broadband white light measurement using NOPA XFROG. The low gain case of a 500 pJ measurement agreed well with a high gain 50 fJ measurement of the same pulse.

The energy per pulse in this case was measured to be 500 pJ. A NOPA XFROG measurement was made for this pulse and the resulting gain was found to be ~ 50. This case was treated as a low gain measurement of the pulse. The pulse was then attenuated by a factor of 10^4 using neutral density filters to yield 50 fJ of energy. The NOPA XFROG trace of this much weaker pulse was measured once more, this time with a higher gain of $\sim$ 1000. The intensity and phase from the two cases were compared to each other as seen in figure(31). The comparison showed that the phases matched extremely well in both cases showing that there was no distortion to the spectral phase during the OPA process. The overall intensity shaped matched well in both cases as well. The structure seen within the envelope of the pulses show similar behavior although they are not identical.

The Group Delay Mismatch (GDM) in the 2-mm thick crystal over the broad bandwidth was minimized and calculated to be 100 fs over the nearly 60-nm spectral envelope FWHM of a 860-fs long (temporal envelope FWHM) pulse. A thinner crystal would further reduce the GDM, but at the same time a compromise would have to be made on the gain that can be achieved. In this demonstration, we used a 2-mm thick Type I crystal to be able to measure 50 fJ weak broadband pulses. Geometrical smearing effects in both the longitudinal and transverse directions were calculated to be 32-fs and 20-fs respectively for the non-collinear geometry.

As an aside, it must be pointed out that the structure in the retrieved white light continuum is real and is the nature of white light continuum generated by nonlinear optical processes. This structure would not be observed in direct spectral measurements using spectrometers for two reasons: The continuum generation process is extremely sensitive to the intensity fluctuations from the amplifier used to generate the continuum. Since the amplifier output is inherently not very stable, the continuum itself varies from shot-to-shot. The time averaging performed over a multishot spectral measurement would wash this structure out. If however, a single-shot measurement were to be performed, the structure in the spectrum would still be unobserved. This is because the white light continuum from the sapphire plate was collected from multiple filaments, in order to duplicate the spatial behavior of broadband fluorescence. Spatial incoherence would thus wash out the spectral

structure in a single shot measurement as well. Our OPA XFROG measurements retrieved a typical spectrum of the broadband continuum.

This ability of the XFROG algorithm to retrieve spectral features which are not revealed by independent spectral measurements has been demonstrated in other broadband continuum measurements of spatially coherent broadband white light [24, 22]. In those cases, single shot spectral measurements revealed that the XFROG retrieved structure was indeed real and that the algorithm was robust. In addition, numerical simulations of broadband continua also indicate that the high order nonlinear processes involved in white light generation cause the spectra to be highly structured [21, 18].

5.3 Theoretical simulations of (N)OPA XFROG

Additional work has been performed in modelling OPA XFROG and its cousin DFG XFROG in order to better understand the thin line between achieving maximum accuracy and maximum efficiency in our measurements. Specifically, we need to minimize the group-delay mismatch (GDM) in the crystal between the two (or three) pulses involved in order to minimize geometrical smearing of the temporal features of the pulse to be measured, in order to make accurate measurements. On the other hand, for the process to be extremely efficient we would have to maximize the gain in the OPA or DFG crystal.

The theoretical simulations were performed by matching the group velocities of the three pulses for typical gains matching experimental conditions. They showed that matching group velocity yielded excellent accuracy with large bandwidths even in the presence of high gains. These simulations looked at the effect of crossing angle α on the OPA XFROG retrieval. As expected for collinear geometry, the retrieved bandwidth was very narrow, $\sim$ 15 nm. Similarly for very large crossing angles $> 8^\circ$ the retrieved bandwidth was again very narrow. Thus, choosing the right crossing angle is imperative in mitigating the effects of beam walk-off.

The simulations also studied the effect of crystal thickness on the retrievals. Thicker crystals required low pump energies in order to avoid pump depletion resulting in lower gains. The distortions caused by GVD for thick crystals could not be neglected. For thin

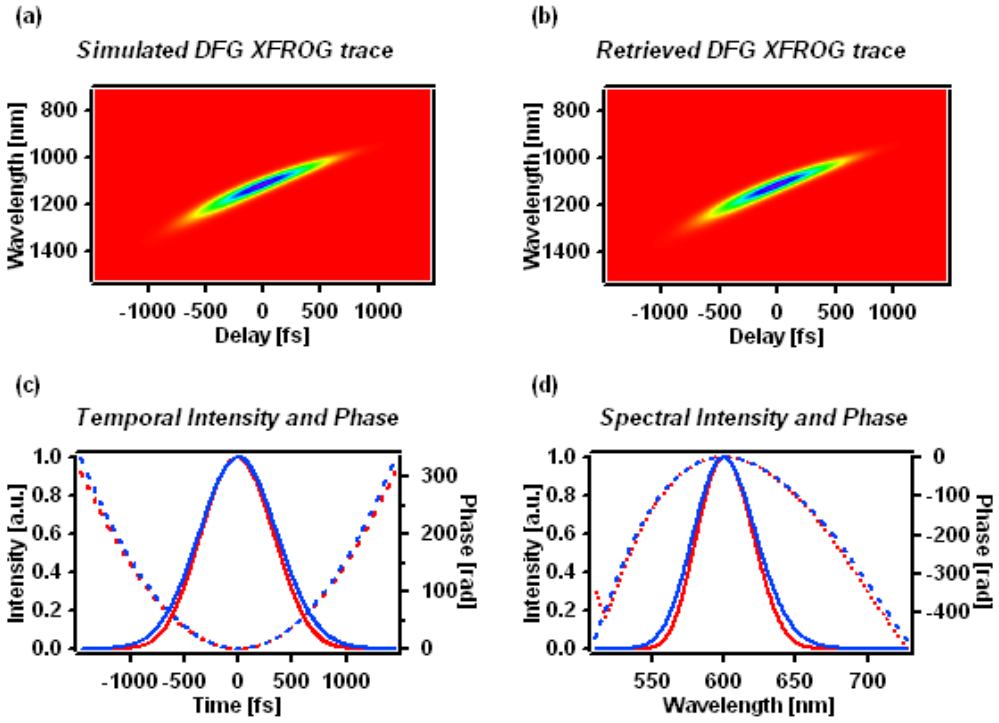

Figure 32: DFG XFROG Trace of a theoretically simulated pulse and its retrieval using a 2-mm thick Type I BBO crystal, with a FROG error of 0.00059. The blue and red colored lines are the theoretical pulses and their corresponding retrievals. The solid lines refer to intensities and the dashed lines, the phases.

crystals, while the distortions from GVD were small, a high pump was required to see significant gains. In all these cases, surprisingly, the spectral phase was always accurately retrieved.

Finally the theoretical simulations looked at one feature of the experiment that was neglected. We claimed that OPA and DFG XFROG processes were similar, so that measuring either of the two signals by spectrally resolving them would yield the unknown pulse by using the correct algorithm. Theoretical simulations simulations of the broadband pulse using a NOPA XFROG geometry confirmed that this was exactly true.

These theoretical simulations were modelled by my colleague Ms. Xuan Liu and the plot in figure(32) was provided by her.

5.4 Conclusion

In the last two chapters, we discussed a new FROG technique that we developed, called OPA XFROG, which, along with its cousin DFG XFROG, is the most sensitive ultrashort-light-pulse-measurement technique now available. Unlike interferometric methods, it does not carry prohibitively restrictive requirements, such as perfect mode-matching, perfect spatial coherence, highly stable absolute phase, and an overlapping-spectrum reference pulse. We have shown that, while care must be taken to avoid GVM effects in such measurements for fs pulses, this problem can be solved by using appropriate broadband crossed-beam geometries. This makes OPA and DFG XFROG powerful tools for measuring non-laser ultrashort light pulses.

We demonstrated that OPA XFROG can measure the intensity and phase vs. time of pulses with only a few attojoules of energy per pulse and with pulse widths on the order of 250 fs and narrow spectra; we have also shown that much broader-band pulses of 850 fs with better than 60 nm of bandwidth can also be measured accurately. Increasing the pump power increases the gain in the process but also increases the background OPG which might make the measurement impractical. Crystal thicknesses have to be chosen carefully in order to minimize distortions due to GVD. It is also necessary to choose the crossing angle between the pump and seed in order to minimize the distortions. DFG XFROG has the same sensitivity and should be ideal for measuring light pulses in the infrared.

With this technique, it should now be possible to use OPA XFROG to measure ultraweak ultrafast light from any general ultrashort light source.

CHAPTER 6

CONCLUSIONS

In this thesis, I studied several schemes to solve the problem of measuring ultraweak arbitrary ultrashort pulses.

In Chapter 2, I demonstrated an alternate scheme to SHG FROG by replacing the beam-splitter with an etalon in order to remove the direction-of-time ambiguity that is present in SHG FROG retrievals. This new variation of FROG is called POLKADOT FROG. A slight variation of POLKADOT FROG, where instead of the beam-splitter, the etalon is placed in the beam path before the pulse enters the FROG device which allows the device to be calibrated easily and painlessly.

The first technique that I looked into for solving the problem of weak pulse measurement, Spectral Interferometry, has been in existence for about 10 years now [19]. As discussed in Chapter 3, in order to make this technique more user-friendly, I demonstrated a scheme that would make it alignment-free. I was able to show that by replacing the slit of the spectrometer by a pin-hole the size of about the order of the wavelength used, it is possible to grossly mis-align the SI experiment by as much as 32° and still make an accurate measurement of the pulses. I was able to demonstrate that long broadband pulses could be retrieved using this alignment-free scheme, subject to the spectral resolution of the spectrometer. Replacing the conventional spectrometer by a fiber spectrometer suggested that the SI experiment could itself be done using fiber-couplers. The fiber-core would act as the pinhole to couple the light in. Using a 2×2 coupler would allow the implementation of an alignment-free Differential Spectral Interferometer, wherein I could measure the interferometric spectrum and it's π-shifted spectrum. This would allow the DC background to be removed from the measurement, while doubling the signal of interest. I have implemented this scheme in conjunction with a Fourier-transform based retrieval algorithm. In

addition I have explored and demonstrated the feasibility of using Dual Quadrature Spectral Interferometry, a less computationally intensive but equally robust algorithm to speed up the inversion. This advancement should prove to be a great boon to the pulse-shaping community which requires easy experimental set-up and immediate feed-back. In addition because the technique results in a signal at only the true delay in the time domain, this opens up the entire temporal range or alternately the full use of the spectral resolution of the spectrometer. This allows for measurement of pulses twice as long as those measured using Fourier Transform based TADPOLE techniques.

I explored Spectral Interferometry for measuring general ultrashort pulses. In particular, I used ultrashort fluorescence as a model for my arbitrary weak light source. Coherence constraints in the nature of the light source as well as the nature of the broadband continuum generated in microstructure fibers, which I intended to use as my reference pulse made me abandon spectral interferometry as a suitable general technique for such measurements.

The pulse energies of these generalized light sources was the main reason that FROG or other typical pulse measurement techniques could not be applied to measure such pulses. Difference Frequency Generation(DFG) is the only (second order) nonlinearity which produces large - exponential gains during the interaction of three pulses in a nonlinear crystal. Optical Parametric Amplification (OPA) is a process that occurs simultaneously with DFG, and shows similar magnitude of gains. I developed the technique of OPA XFROG to measure extremely weak pulses. In Chapter 4, I demonstrated the reliability of the technique by comparing OPA XFROG measurements of a fairly weak 250 fs long pulse around 600 nm, with the well-established technique of Sum Frequency Generation (SFG) XFROG. Already in the demonstration, OPA XFROG was able to do three orders of magnitude better than the SFG XFROG measurement, in measuring a pulse that was a 1000 times weaker. I then went on to demonstrate the measurement of a pulse of about 150 aJ using the OPA XFROG technique. At this point, I ran into limitations due to the presence of super-fluorescence background which rivalled the signal I was trying to measure. The intensity signal-to-noise in this measurement was a factor of 5 on the CCD camera. However this attojoule pulse had experienced a gain of about 5000 during the OPA process, which made it necessary to

attenuate my signal before it entered the spectrometer before it was spectrally resolved.

In Chapter 5, I studied another aspect of the problem of measuring ultraweak fluorescence-like pulses. Even though these pulses are about the order of 1-2 picoseconds, these pulses have very large bandwidths. In order to be able to measure such pulses not only would I need to amplify them, but I would also need to phase-match such large bandwidths simultaneously. I showed that by going to a non-collinear geometry, a NOPA XFROG, it was possible to phase-match large bandwidths, in excess of 100 nm. In the experimental demonstration, I imposed a limit on the bandwidth to $\sim$ 60 nm with the use of two neutral density filters and made a measurement of such broadband pulses. I briefly discussed the effect of Group Velocity Mismatch on such a measurement. Further theoretical work on this problem has been done by my colleague, Ms. Xuan Liu, to make sure that the NOPA XFROG does indeed retrieve the phase of the pulse accurately.

Based on these theoretical considerations and my experimental work, NOPA XFROG appears to be an ideal choice for measuring broadband ultraweak ultrashort pulses. I look forward to the technique being used to make such measurements and opening up new vistas of knowledge in the future.

APPENDIX A

DERIVATION OF THE 50 % REQUIREMENT FOR THE FIRST SURFACE OF THE ETALON IN POLKADOT FROG

This appendix originally appeared as an appendix in the paper by the author:

E. Zeek, A. P. Shreenath, P. O'Shea, M. Kimmel, and R. Trebino, "Simultaneous automatic calibration and direction-of-time removal frequency-resolved optical gating," Applied Physics B-Lasers and Optics 74, S265-S271 (2002). [45]

In Chapter 2, we have used the fact that only the first surface of the etalon needs to have s 50% reflectivity. It is not obvious that only the first surface is restricted and that the second surface is unrestricted. To perform a FROG measurement the two pulses must have identical shapes, but they can differ by a multiplicative factor without adversely affecting the measurement. Given the schematic in figure(33), the following equations can be written for the two pulse trains:

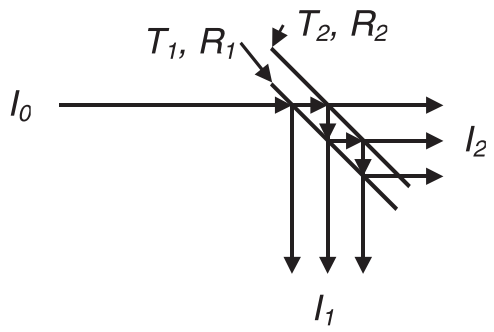

Figure 33: Etalon Schematic. This is an exaggerated diagram of an etalon. The input beam, I_0, bounces between the two partially reflective surfaces. Each round-trip creates an attenuated, delayed replica of the input pulse.

$$\begin{aligned} I_1 &= \left(R_1 + T_1R_2T_1 + T_1R_2R_1R_2T_1 + T_1R_2\left(R_1R_2\right)^2T_1 + \cdots\right)I_0 \\ I_2 &= \left(T_2T_1 + T_2R_1R_2T_1 + T_2\left(R_1R_2\right)^2T_1 + T_2\left(R_1R_2\right)^3T_1 + \cdots\right)I_0 \end{aligned} \tag{38}$$

where T_i and R_i are the transmission and reflectivities, respectively, of the first and second surfaces, I_0 is the input intensity, and I_1 and I_2 are the transmitted intensities. We have not explicitly shown the delay factor in these equations; each element in the sum represents a pulse separated by τ_{sep} from its neighbors. Factoring eqn. (38) yields:

$$\begin{aligned} \tfrac{I_1}{I_0} &= R_1\left(1 + \tfrac{T_1^2R_2}{R_1}\left(\sum_{i=0}^{\infty}\left(R_1R_2\right)^i\right)\right) \\ \tfrac{I_2}{I_0} &= T_1T_2\left(1 + R_1R_2\left(\sum_{i=0}^{\infty}\left(R_1R_2\right)^i\right)\right) \end{aligned} \tag{39}$$

The R_1 and T_1T_2 terms are unimportant for our purposes (They represent multiplicative factors.). This means that, for both pulses to have the same shape, the following must hold true:

$$1 + \frac{T_1^2R_2}{R_1}\left(\sum_{i=0}^{\infty}\left(R_1R_2\right)^i\right) = 1 + R_1R_2\left(\sum_{i=0}^{\infty}\left(R_1R_2\right)^i\right) \tag{40}$$

.

From this equation, it is evident that the important factors are before the sum:

$$\frac{T_1^2R_2}{R_1} = R_1R_2 \tag{41}$$

.

This yields the following condition:

$$T_1 = R_1 \tag{42}$$

.

The only parameters remaining pertain to the first surface. For a lossless interface, , simplifying eqn. (42) to:

$$\begin{aligned} R_1 &= 1 - R_1 \\ R_1 &= 1\!/\!_2 \end{aligned} \tag{43}$$

.

Therefore, if the first surface has a reflectivity of 50%, both pulses trains are identical.

REFERENCES

[1] Baltuska, A., Pshenichnikov, M., and Wiersma, D., "Amplitude and phase characterization of 4.5 fs pulses by frequency-resolved optical gating," *Opt. Lett.*, vol. 23, no. 18, pp. 1474–6, 1998.

[2] Blit, S., Weaver, E. G., and Tittel, F. K., "Wavelength temperature and angle bandwidths in shg of focused beams in non-linear crystals," *Applied Optics*, vol. 18, no. 5, pp. 733–736, 1979. Article Gl728 English Times Cited:4 Cited References Count:11.

[3] Bloembergen, N., *Nonlinear Optics*. New York: W.A. Benjamin, 1965.

[4] Born, M. and Wolf, E., *Principles of Optics*. Cambridge, UK: University Press, Cambridge, seventh (expanded) ed., 2002.

[5] Boyd, G. D, K. D. A., "Parametric interaction of focused gaussian light beams," *Journal of Applied Physics*, vol. 39, no. 8, pp. 3597–3639, 1968.

[6] Boyd, R. W., *Nonlinear Optics*. Academic Press, second ed., 2003.

[7] Cerullo, G. and De Silvestri, S., "Ultrafast optical parametric amplifiers," *Review of Scientific Instruments*, vol. 74, no. 1, pp. 1–18, 2003. Times Cited: 4 Cited Reference Count: 133 English Review REV SCI INSTR Part 1 636JL.

[8] Cerullo, G., Nisoli, M., Stagira, S., and Silvestri, S., "Sub-8-fs pulses from an ultrabroadband optical parametric amplifier in the visible," *Opt. Lett.*, vol. 23, no. 16, p. 1283, 1998.

[9] Choma, M. A., Yang, C. H., and Izatt, J. A., "Instantaneous quadrature low-coherence interferometry with 3 x 3 fiber-optic couplers," *Optics Letters*, vol. 28, no. 22, pp. 2162–2164, 2003. Article 740AR English Times Cited:4 Cited References Count:10.

[10] Danielius, R., Dubietis, A., Piskarskas, A., Valiulis, G., and Varanavicius, A., "Generation of compressed 600-720-nm tunable femtosecond pulses by transient frequency mixing in a beta-barium borate crystal," *OPTICS LETTERS*, vol. 21, no. 3, pp. 216–218, 1996. Article TU233 English Times Cited:14 Cited References Count:9.

[11] Danielius, R., Piskarskas, A., Di Trapani, P., Andreoni, A., Solcia, C., and Foggi, P., "A collinearly phase-matched parametric generator/amplifier of visible femtosecond pulses," *IEEE JOURNAL OF QUANTUM ELECTRONICS*, vol. 34, no. 3, pp. 459–464, 1998. Article YZ366 English Times Cited:9 Cited References Count:20.

[12] Danielius, R., Piskarskas, A., DiTrapani, P., Andreoni, A., Solcia, C., and Foggi, P., "Matching of group velocities by spatial walk-off in collinear three-wave interaction with tilted pulses," *OPTICS LETTERS*, vol. 21, no. 13, pp. 973–975, 1996. Article UU284 English Times Cited:32 Cited References Count:12.

[13] Danielius, R., Piskarskas, A., DiTrapani, P., Andreoni, A., Solcia, C., and Foggi, P., "Visible pulses of 100 fs and 100 mu j from an upconverted parametric generator," *APPLIED OPTICS*, vol. 35, no. 27, pp. 5336–5339, 1996. Article VF926 English Times Cited:24 Cited References Count:14.

[14] DeLong, K., Trebino, R., and Kane, D., "Comparison of ultrashort-pulse frequency-resolved-optical-gating traces for three common beam geometries," *J. Opt. Soc. Amer. B*, vol. 11, no. 9, pp. 1595–1608, 1994.

[15] Dorrer, C., Belabas, N., Likforman, J. P., and Joffre, M., "Spectral resolution and sampling issues in fourier-transform spectral interferometry," *Journal of the Optical Society of America B-Optical Physics*, vol. 17, no. 10, pp. 1795–1802, 2000. Times Cited: 20 Cited Reference Count: 35 English Article J OPT SOC AM B-OPT PHYSICS 363JK.

[16] Dorrer, C. and Joffre, M., "Characterization of the spectral phase of ultrashort light pulses," *Comptes Rendus De L Academie Des Sciences Serie Iv Physique Astrophysique*, vol. 2, no. 10, pp. 1415–1426, 2001. Times Cited: 4 Cited Reference Count: 67 English Article C R ACAD SCI SER IV-PHYS ASTR 523RJ.

[17] Dreger, M. A. and Mciver, J. K., "2nd-harmonic generation in a nonlinear, anisotropic medium with diffraction and depletion," *Journal of the Optical Society of America B-Optical Physics*, vol. 7, no. 5, pp. 776–784, 1990. Article De180 English Times Cited:14 Cited References Count:18.

[18] Dudley, J. M., Gu, X., Xu, L., Kimmel, M., Zeek, E., O'Shea, P., Trebino, R., Coen, S., and Windeler, R. S., "Cross-correlation frequency resolved optical gating analysis of broadband continuum generation in photonic crystal fiber: simulations and experiments," *Optics Express*, vol. 10, no. 21, pp. 1215–1221, 2002. Times Cited: 0 Cited Reference Count: 16 English Article 606QV OPT EXPRESS.

[19] Fittinghoff, D., Bowie, J., Sweetser, J., Jennings, R., Krumbgel, M., DeLong, K., Trebino, R., and Walmsley, I., "Measurement of the intensity and phase of ultraweak, ultrashort laser pulse," *Optics Letters*, vol. 21, no. 12, pp. 884–886, 1996. TADPOLE.

[20] Froehly, C., Lacourt, A., and Vienot, J. C., "Time impulse response and time frequency response of optical pupils. experimental confirmations and applications," *Nouvelle Revue D'Optique*, vol. 4, pp. 183–96, 1973.

[21] Gaeta, A. L., "Nonlinear propagation and continuum generation in microstructured optical fibers," *Optics Letters*, vol. 27, no. 11, pp. 924–926, 2002. ISI Document Delivery No.: 556VU English 0146-9592.

[22] Gu, X., Akturk, S., Shreenath, A., Cao, Q., and Trebino, R., "The measurement of ultrashort light pulses - simple devices, complex pulses," *Optical Review*, vol. 11, no. 3, pp. 141–152, 2004. Review 844XE English Times Cited:0 Cited References Count:54.

[23] Gu, X., Kimmel, M., Shreenath, A. P., Trebino, R., Dudley, J. M., Coen, S., and Windeler, R. S., "Experimental studies of the coherence of microstructure-fiber

supercontinuum," *Optics Express*, vol. 11, no. 21, pp. 2697–2703, 2003. Times Cited: 5 Cited Reference Count: 15 English Article OPT EXPRESS 734EH.

[24] Gu, X., Xu, L., Kimmel, M., Zeek, E., O'Shea, P., Shreenath, A. P., Trebino, R., and Windeler, R. S., "Frequency-resolved optical gating and single-shot spectral measurements reveal fine structure in microstructure-fiber continuum," *Optics Letters*, vol. 27, no. 13, pp. 1174–1176, 2002. Times Cited: 2 Cited Reference Count: 6 English Article 569VM OPTICS LETTERS.

[25] Kane, D. J., "Real-time measurement of ultrashort laser pulses using principal component generalized projections," *IEEE Journal of Selected Topics in Quantum Electronics*, vol. 4, no. 2, pp. 278–84, 1998.

[26] Krylov, V., Gallus, J., Wild, U. P., Kalintsev, A., and Rebane, A., "Femtosecond noncollinear and collinear parametric generation and amplification in bbo crystal," *Applied Physics B-Lasers and Optics*, vol. 70, no. 2, pp. 163–168, 2000. Article 295FK English Times Cited:6 Cited References Count:15.

[27] Lepetit, L. and Joffre, M., "Two-dimensional nonlinear optics using fourier-transform spectral interferometry," *Opts. Lett.*, vol. 21, no. 8, pp. 564–566, 1996. Tadpole application.

[28] Linden, S., Giessen, H., and Kuhl, J., "Xfrog-a new method for amplitude and phase characterization of weak ultrashort pulses," *Physica Status Solidi B Conference Title: Phys. Status Solidi B (Germany)*, vol. 206, no. 1, pp. 119–24, 1998.

[29] Linden, S., Kuhl, J., and Giessen, H., "Amplitude and phase characterization of weak blue ultrashort poulses by downconversion," *Opt. Lett.*, vol. 24, no. 8, pp. 569–71, 1999. XFROG.

[30] Louisell, W. H., Siegman, A. E., and Yariv, A., "Quantum fluctuations and noise in parametric processes.1.," *Physical Review*, vol. 1, no. 6, p. 1646. Article 1461C.

[31] O'Shea, P., Kimmel, M., Gu, X., and Trebino, R., "Highly simplified ultrashort pulse measurement," *Opt. Lett.*, vol. 26, p. 932, 2001.

[32] Piasecki, J., Colombeau, B., Vampouille, M., Froehly, C., and Arnaud, J., "Nouvelle mthode de mesure de la rponse impulsionnelle des fibres optiques," *Appl. Opt.*, vol. 19, no. 22, pp. 3749–3755, 1980. Spectral interferometry.

[33] Ranka, J. K., Windeler, R. S., and Stentz, A. J., "Visible continuum generation in air-silica microstructure optical fibers with anomalous dispersion at 800 nm," *Opt. Lett.*, vol. 25, no. 1, pp. 25–7, 1999.

[34] Riedle, E., Beutter, M., Lochbrunner, S., Piel, J., Schenkl, S., Sporlein, S., and Zinth, W., "Generation of 10 to 50 fs pulses tunable through all of the visible and the nir," *APPLIED PHYSICS B-LASERS AND OPTICS*, vol. 71, no. 3, pp. 457–465, 2000. Article 352GW English Times Cited:45 Cited References Count:47.

[35] Shen, Y., *The Principles of Nonlinear Optics*. New York: John Wiley and Sons, 1984.

[36] Smith, A. V., "Snlo nonlinear optics code, sandia national laboratories."

[37] Smith, A., "Group-velocity-matched three-wave mixing in birefringent crystals," *OPTICS LETTERS*, vol. 26, no. 10, pp. 719–721, 2001. Article 431FZ English Times Cited:6 Cited References Count:8.

[38] Trebino, R., *Frequency-Resolved Optical Gating: The Measurement of Ultrashort Laser Pulses*. Boston: Kluwer Academic Publishers, 2000.

[39] Trebino, R., DeLong, K., Fittinghoff, D., Sweetser, J., Krumbgel, M., and Kane, D., "Measuring ultrashort laser pulses in the time-frequency domain using frequency-resolved optical gating," *Review of Scientific Instruments*, vol. 68, no. 9, pp. 3277–3295, 1997.

[40] Trebino, R. and Kane, D., "Using phase retrieval to measure the intensity and phase of ultrashort pulses: Frequency-resolved optical gating," *J. Opt. Soc. Amer. A*, vol. 10, no. 5, pp. 1101–1111, 1993.

[41] Vakhtin, A. B., Peterson, K. A., Wood, W. R., and Kane, D. J., "Differential spectral interferometry: an imaging technique for biomedical applications," *Optics Letters*, vol. 28, no. 15, pp. 1332–1334, 2003. Article 702ZZ English Times Cited:3 Cited References Count:10.

[42] van Cittert, P. H. *Physica*, vol. 1, p. 201, 1934.

[43] Walmsley, I. A. and Wong, V., "Characterization of the electrical field of ultrashort optical pulses," *J. Opt. Soc. Am. B*, vol. 13, no. 11, pp. 2453–2463, 1996. Ian's definitive theory of pulse-measurement techniques. In this analysis, FROG is the best-known variant of a Type I (amplitude time-nonstationary–amplitude stationary) device.

[44] Wong, V. and Walmsley, I., "Analysis of ultrashort pulse-shape measurement using linear interferometers," *Optics Letters*, vol. 19, no. 4, pp. 287–289, 1994. Shows that linear methods don't work for ultrashort pulses.

[45] Zeek, E., Shreenath, A. P., O'Shea, P., Kimmel, M., and Trebino, R., "Simultaneous automatic calibration and direction-of-time removal frequency-resolved optical gating," *Applied Physics B-Lasers and Optics*, vol. 74, pp. S265–S271, 2002. Times Cited: 0 Cited Reference Count: 5 Cited References: KANE DJ, 1993, OPT LETT, V18, P823 OSHEA P, 2001, OPT LETT, V26, P932 TAFT G, COMMUNICATION TREBINO R, 1993, J OPT SOC AM A, V10, P1101 TREBINO R, 1997, REV SCI INSTRUM, V68, P3277 English Article S 590GY APPL PHYS B-LASERS OPT.

[46] Zernike, F. *Physica*, vol. 5, p. 785, 1938.

[47] Zhang, J. Y., H. J. Y. and Shen, Y. R., "Optical parametric generation and amplification," in *An International Handbook on Laser Science and Technology* (Lectokhov, V. S., S. C. V. S. Y. R. and Walther, H., eds.), Hardwood Academic Publishers, 1995.

[48] Zhang, J. Y., Shreenath, A. P., Kimmel, M., Zeek, E., Trebino, R., and Link, S., "Measurement of the intensity and phase of attojoule femtosecond light pulses using optical-parametric-amplification cross-correlation frequency-resolved optical gating," *Optics Express*, vol. 11, no. 6, pp. 601–609, 2003. Times Cited: 1 Article English Cited References Count: 19 659ez.

VITA

Aparna Prasad Shreenath, née Aparna Prasad, was born in Mysore in South India in 1973. Inspired by popular science programs on TV and Jules Verne's *Journey through the center of the earth*, she majored in Physics, Mathematics and Geology, to obtain her Bachelor of Science degree from the University of Mysore, India in 1995. She went on to get a Master of Science in Physics from the University of Mysore in 1997. She came to the School of Physics at Georgia Institute of Technology in 1997 to pursue graduate studies and joined the Ultrafast Optics group under Rick Trebino in the summer of 1999. She obtained her Master of Science from the College of Engineering for course-work in Electrical Engineering in 2002. She lives in Marietta, GA and is married to Jay Shreenath since February of 1998. She is eagerly awaiting the arrival of their first child in October, 2005.